

1 **Cancer-associated HIF-2 α impacts trunk neural crest stemness**

2

3 Sofie Mohlin^{a,b,c,*}, Camilla U. Persson^{b,1}, Elina Fredlund^{a,b,1}, Emanuela Monni^{d,e}, Jessica M.
4 Lindvall^f, Zaal Kokaia^{d,e}, Emma Hammarlund^b and Marianne E. Bronner^c

5

6 ^a Division of Pediatrics, Department of Clinical Sciences, Lund University, Lund, Sweden.

7 ^b Translational Cancer Research, Lund University Cancer Center at Medicon Village, Lund
8 University, Lund, Sweden.

9 ^c Division of Biology and Biological Engineering, California Institute of Technology,
10 Pasadena, CA, 91125, USA.

11 ^d Laboratory of Stem Cells and Restorative Neurology, University Hospital, Lund, Sweden.

12 ^e Lund Stem Cell Center, Lund University, Lund, Sweden.

13 ^f Jessica M. Lindvall, National Bioinformatics Infrastructure Sweden (NBIS), Science for Life
14 Laboratory, Department of Biochemistry and Biophysics, Stockholm University, S-10691
15 Stockholm, Sweden.

16

17 ¹These authors contributed equally to this work

18

19 *Correspondence to: Sofie Mohlin; sofie.mohlin@med.lu.se. Translational Cancer Research;
20 Division of Pediatrics, Lund University Cancer Center, Lund, Sweden.

21

22 **Abstract**

23 The neural crest is a stem cell population that gives rise to sympathetic ganglia, the cell type of
24 origin of neuroblastoma. Hypoxia Inducible Factor (HIF)-2 α is associated with high risk
25 neuroblastoma, however, little is known about its role in normal neural crest development. To
26 address this important question, here we show that HIF-2 α is expressed in trunk neural crest
27 cells of human, murine and avian embryos. Modulating HIF-2 α *in vivo* not only causes
28 developmental delays but also induces proliferation and stemness of neural crest cells while
29 altering the number of cells migrating ventrally to sympathoadrenal sites. Transcriptome
30 changes after loss of HIF-2 α reflect the *in vivo* phenotype. The results suggest that expression
31 levels of HIF-2 α must be strictly controlled and abnormal levels increase stemness and may
32 promote metastasis. Our findings help elucidate the role of HIF-2 α during normal development
33 with implications also in tumor initiation at the onset of neuroblastoma.

34

35 **Key words:** Neural crest, trunk neural crest, neuroblastoma, hypoxia inducible factor-2, HIF,
36 chick embryo

37

38 **Introduction**

39 The neural crest is a multipotent stem cell population that is unique to vertebrate embryos.
40 Originating from the ectodermal germ layer, premigratory neural crest cells arise in the dorsal
41 neural tube during neurulation and are characterized by expression of transcription factors like
42 *FOXD3*, *TFAP2* and *SOXE* (Khudyakov & Bronner-Fraser, 2009). Neural crest cells
43 subsequently undergo an epithelial-to-mesenchymal transition (EMT) to delaminate from the
44 neuroepithelium, then migrate extensively throughout the embryo, populating distant sites.
45 Upon reaching their final destinations, neural crest cells form a large variety of cell types, as
46 diverse as elements of the craniofacial skeleton, melanocytes of the skin, adrenal chromaffin
47 cells and sympathetic neurons and glia (Ayer-Le Lievre & Le Douarin, 1982; Bittencourt, da
48 Costa, Calloni, Alvarez-Silva, & Trentin, 2013; Bronner-Fraser & Fraser, 1988; Vega-Lopez,
49 Cerrizuela, Tribulo, & Aybar, 2018).

50

51 The stem cell properties and migratory nature of the neural crest are highly reminiscent of tumor
52 cells. Indeed, many of the genes involved in neural crest EMT are redeployed in metastatic
53 cancers including many types of neural crest-derived cancers. Thus, neural crest cells represent
54 an excellent model for studying the origin of neural crest-derived tumors including pediatric
55 neuroblastoma, a tumor of infancy responsible for 15% of all cancer-related deaths in children
56 (Maris, 2010). Neuroblastoma patients are very young, with some tumors detected in newborns.
57 It is well accepted that neuroblastoma derives from sympathetic neuroblasts that originate from
58 trunk neural crest cells (De Preter et al., 2006; Hoehner et al., 1996).

59

60 High risk neuroblastoma correlates with the presence of cells in perivascular niches (Pietras et
61 al., 2008) that express high levels of Hypoxia Inducible Factor (HIF)-2 α together with
62 numerous neural crest markers (Holmquist-Mengelbier et al., 2006; Pietras et al., 2008; Pietras

63 et al., 2009). Under normal conditions, HIF-2 α is stabilized at low oxygen levels and responds
64 to hypoxia by initiating a transcriptional program for cellular adaptation to changes in metabolic
65 demand. In neuroblastoma, however, HIF-2 α becomes abnormally stabilized at physiological
66 oxygen tensions (~5% O₂) (Holmquist-Mengelbier et al., 2006). This, together with the
67 presence of neural crest markers in neuroblastoma tumors, raises the intriguing possibility that
68 HIF-2 α expressing neural crest cells in the early embryo might reflect the cell type of origin in
69 tumor initiation.

70

71 Here, we explore this possibility by examining the role of HIF-2 α , encoded by the gene *EPAS1*,
72 during normal neural crest development and possible correlations with neuroblastoma. We
73 show that HIF-2 α is expressed in migrating trunk neural crest and sympathetic neuroblasts in
74 human, murine and avian embryos. RNA sequencing of trunk neural crest cells with
75 dysregulated HIF-2 α levels demonstrates a shift in the global transcriptional program, resulting
76 in enrichment in genes associated with processes connected to tumor morphology, invasion,
77 EMT and arrested embryo growth. Perturbation experiments in chick embryos *in vivo* result in
78 a delay in embryonic growth, altered expression of trunk neural crest genes, and disrupted trunk
79 neural crest cell migration. Consistent with this, *in vitro* crestospheres display increased
80 proliferation and self-renewal capacity. The results suggest that expression levels of HIF-2 α
81 must be tightly regulated. These findings enhance our understanding of how genes dysregulated
82 in normal development may result in onset of neuroblastoma.

83

84

85 **Results**

86 *HIF-2 α is expressed in migratory trunk neural crest cells in chick embryos*

87 The presence of neuroblastoma cells expressing hypoxia inducible factor (HIF)-2 α in
88 perivascular tumor niches indicates poor prognosis in this tumor form. That these cells express
89 stem cell- and neural crest associated proteins raises the intriguing possibility that they may
90 constitute a tumor-initiating subpopulation of cells that resembles embryonic neural crest cells.
91 HIF-2 α is a transcription factor that localizes to the nucleus but also is found in the cytoplasm
92 (Holmquist-Mengelbier et al., 2006; Mohlin, Hamidian, & Pahlman, 2013), though its role in
93 the cytoplasm remains unknown. Consistent with this dual localization, Western blots of stage
94 HH18 wild type chick embryos revealed expression of HIF-2 α in both the nuclear and
95 cytoplasmic fractions (**Figure 1A**), similar to what has been observed in oxygenated
96 neuroblastoma cells (Holmquist-Mengelbier et al., 2006).

97 As a first step in exploring the role of HIF-2 α in the embryo, we examined its spatiotemporal
98 expression during normal neural crest development. To this end, RNA was extracted from
99 whole chick embryos from stages HH4 to HH27, reflecting stages from gastrulation to mid-
100 gestation. The results revealed continuous expression of HIF-2 α (encoded by the gene *EPAS1*)
101 over the time course analyzed, with a peak at HH18 which reflects the time of active trunk
102 neural crest migration (**Figure 1B**). Next, we performed immunocytochemistry with an
103 antibody against HIF-2 α in transverse sections through the trunk region of stage HH11, HH13
104 and HH18 embryos. We detected HIF-2 α protein in scattered neural crest cells within the neural
105 tube of HH11 and HH13 embryos, stages when trunk neural crest cells are still premigratory
106 (**Figure 1C-D**, respectively). We further detected HIF-2 α in trunk neural crest cells that had
107 delaminated from the neural tube and initiated migration (**Figure 1E-F**). Possible non-specific
108 binding by the primary antibody was ruled out by secondary antibody only staining

109 **(Supplementary Figure S1A).**

110

111 HIF-2 α is canonically induced at low oxygen levels. To understand variations in oxygen
112 consumption during the developmental stages of interest, we measured O₂ saturation in real-
113 time in the developing chick embryo utilizing a microsensors technique (**Figure 1G**). Within the
114 trunk neural tube, oxygen saturation starts out high (up to 85% \pm 5 SEM O₂ saturation) at
115 premigratory to migratory stages of neural crest development (HH10 – HH16) and gradually
116 decreases (**Figure 1G**). At the time when the majority of trunk neural crest cells have
117 delaminated from the tube (HH18), oxygen saturation is low (23% \pm 10 SEM O₂ saturation),
118 only to rise at later time points (**Figure 1G**). Together with the expression data above, the
119 results suggest that HIF-2 α is independent of oxygen availability in the developing embryo
120 (**Figure 1C-G and Figure 2**).

121

122 *HIF-2 α is expressed in sympathetic neuroblasts in human and mouse embryos*

123 *EPAS1* knockout mice have severe abnormalities in the sympathetic nervous system (Tian,
124 Hammer, Matsumoto, Russell, & McKnight, 1998); consistent with this, there is some, albeit
125 limited, data suggesting that HIF-2 α is expressed in sympathetic chain ganglia up to murine
126 day E11.5 (corresponding to human embryonic week 5). Moreover, mice lacking *PHD3* (HIF
127 prolyl hydroxylase), a gene critical for regulation of HIF-2 α , display reduced sympathetic
128 nervous system (SNS) function that is rescued by crossing these mutants with *EPAS1*^{+/-} mice
129 (Bishop et al., 2008).

130

131 We have previously shown that HIF-2 α is expressed in sympathetic ganglia of human embryos
132 at embryonic week 6.5 (~E12.5 in mice) but that expression is lost in these cells at later stages
133 (fetal week 8) (Mohlin et al., 2013). Here, we confirmed expression of HIF-2 α in sympathetic
134 ganglia in mouse embryos at E12.5 by staining adjacent sections with HIF-2 α (**Figure 2A**) and
135 TH (**Figure 2B**) antibodies, with the latter indicating the location of sympathetic ganglia.
136 Demonstrating antibody specificity, HIF-2 α expression was only observed in conventional
137 neuroblastoma SK-N-BE(2)c cells cultured at hypoxia (1% O₂) but not normoxia (21% O₂)
138 (**Supplementary Figure S1B**). In sections, we detected HIF-2 α positive cells specifically in
139 the dorsal neural tube, as well as in early neural crest migratory streams in sections through the
140 trunk region of a human embryo of embryonic week ew5 (Carnegie stage 13; **Figure 2C-D**).
141 In contrast, there were virtually no HIF-2 α positive cells left within the neural tube at
142 embryonic week ew6 (Carnegie stage 16). Rather, positive cells could be detected migrating
143 along the ventral pathway followed by sympathoadrenal precursors (**Figure 2E**). Consistent
144 with our biochemical analysis in the chick (**Figure 1A**), human HIF-2 α expression was noted
145 in both the nucleus and cytoplasm (**Figure 2E**).

146

147 *Knockdown of HIF-2 α delays embryogenesis, alters gene expression and affects cell numbers*
148 *along the ventral neural crest migratory pathway*

149 To examine the role of HIF-2 α *in vivo*, we performed loss-of-function experiments in chick
150 embryos using both morpholino-mediated knock-down as well as CRISPR/Cas9 knock-out
151 using three different gRNAs. We then let the embryos develop for an additional one (for gene
152 expression) or two (for staging and migration) days and analyzed several potentially affected
153 biological processes. Surprisingly, we noticed that HIF-2 α knockdown embryos were

154 developmentally delayed compared with their control counterparts (**Figure 3A-D**). The stages
155 of embryos following CRISPR/Cas9- or morpholino mediated loss of HIF-2 α were determined
156 by their Hamburger and Hamilton developmental stage *in ovo* (**Figure 3A-B**) and by counting
157 somites *ex ovo* (**Figure 3C-D**).

158

159 Electroporation efficiency was confirmed by analyzing *EGFP* expression (**Supplementary**
160 **Figure S2A-B**). Knockdown of HIF-2 α , either by morpholino or CRISPR/Cas9, led to
161 decreased expression levels of genes representative of early and migrating neural crest as well
162 as trunk neural crest cells in particular (Frith et al., 2018; Murko, Vieceli, & Bronner, 2018)
163 (**Figure 3E-G**, respectively, and **Supplementary Figure S2C-D**). In contrast, the cranial
164 neural crest associated gene *HOXA2* was not affected (**Figure 3F, H**).

165

166 One of the most important features of neural crest cells is their migratory ability. Trunk neural
167 crest cells destined to form the sympathetic chain ganglia migrate ventrally. After HIF-2 α loss
168 of function using either morpholinos or CRISPR/Cas9, HNK1 positive migratory neural crest
169 cells were detected on the control side in all embryos (**Figure 4A-D**) as well as on the side
170 electroporated with non-targeting gRNA CTRL and control 5'-mismatch morpholino (**Figure**
171 **4A and 4C**, respectively). In contrast, loss of HIF-2 α profoundly reduced the numbers of
172 HNK1 positive cells migrating to ventral regions of the embryo (CRISPR/Cas9, **Figure 4B**;
173 morpholino, **Figure 4D**).

174

175 SOX9, a member of the SoxE family of transcription factors, is important for neural crest fate.
176 It is expressed in premigratory neural crest cells at all axial levels and promotes their lineage

177 progression. Importantly, transverse sections through the trunk of embryos electroporated with
178 control or two different EPAS1 targeting gRNA constructs showed no differences in SOX9
179 expression (**Supplementary Figure S3A-C**), suggesting that neural crest lineage specification
180 was unaffected by loss of HIF-2 α .

181

182 *Over-expression of HIF-2 α has similar effects as loss-of-function*

183 Similar to the loss-of-function experiments, overexpression of HIF-2 α led to delayed
184 embryonic development (**Figure 5A**) and perturbed migration as visualized by HNK1 staining
185 (**Figure 5B**). Expression of neural crest- and trunk specific genes was slightly suppressed
186 (**Figure 5C** and **Supplementary Figure S4A**) whereas expression of cranial neural crest gene
187 *HOXA2* was slightly induced (**Figure 5C**). Overexpression of *EPAS1* was confirmed by qRT-
188 PCR (**Supplementary Figure S4B**).

189

190 *Trunk neural crest cells proliferate extensively in response to dysregulated HIF-2 α*

191 We next examined cell proliferation in premigratory and migrating neural crest cells after loss
192 of HIF-2 α using real-time EdU pulse chase labeling optimized for avian embryos (Warren et
193 al., 2009). Quantifying the proportion of premigratory and early migrating neural crest cells
194 that had incorporated EdU demonstrated a significant induction of proliferating cells with an
195 average proportion of double positive cells of 22% and 70% in the 5'-mismatch versus EPAS1
196 morpholino targeted embryos, respectively (p 0.029; **Figure 6A-B**).

197

198 After over-expression of HIF-2 α , real-time EdU incorporation demonstrated that cells with

199 increased expression of HIF-2 α also became highly proliferative with an average proportion of
200 double positive cells of 11% and 52% in the control and EPAS1 overexpressing embryos,
201 respectively (p 0.011; **Figure 6C-D**). We conclude that neural crest proliferation is highly
202 sensitive to expression levels of HIF-2 α , suggesting that levels must be tightly controlled for
203 proper development.

204

205 *HIF-2 α downregulation enhances stem cell properties of trunk NC cells*

206 Neural crest-derived crestosphere cultures (Mohlin & Kerosuo, 2019; Mohlin, Kunttas, et al.,
207 2019) enable studies on stemness properties of these cells *in vitro*. Therefore, we examined
208 *EPAS1* expression in crestosphere cultures, in which multipotent neural crest cells can be
209 maintained in a stem cell-like state *in vitro* (Kerosuo et al., 2015; Mohlin, Kunttas, et al., 2019).
210 When comparing crestosphere cultures derived from trunk versus cranial axial levels, we noted
211 that *EPAS1* was enriched in trunk crestospheres (**Figure 6E**). *In situ* hybridization further
212 revealed two separate patterns of *EPAS1* expression in trunk crestospheres: equal distribution
213 throughout the spheres or concentration in cells at the edges of the spheres (**Figure 6F**).

214

215 Next, we established trunk crestospheres from embryos electroporated with a control gRNA
216 construct or two different gRNAs targeting *EPAS1*. Primary sphere assays demonstrated that
217 cells with dysregulated HIF-2 α levels had an increased ability to form new spheres when seeded
218 as single cells (1 cell/well; **Figure 6G-H**). In addition, crestosphere cultures derived from
219 embryos electroporated with the *EPAS1* targeting construct formed larger spheres compared to
220 their control counterparts (**Figure 6H**).

221

222 *RNA-seq after loss of HIF-2 α in neural crest cells identifies downstream genes associated with*
223 *invasion, growth arrest and developmental regulation*

224 To investigate gene expression changes after loss of HIF-2 α , we performed loss of function
225 experiments at premigratory stages of neural crest development (HH10⁺/HH11 in avian
226 embryos) using a splice targeting morpholino as above. Neural tubes from trunk region were
227 dissected 24 hours post-electroporation (at stage ~HH16) and subsequently analyzed by RNA
228 sequencing. Correlation plot of all genes from the dataset demonstrated that trunk neural crest
229 cells after knockdown of HIF-2 α indeed differ from those injected with control scrambled
230 morpholino (spearman $p > 0.96$; **Figure 7A**). Setting a cut-off at $p < 0.005$ and removing all hits
231 that were not annotated (NA), we identified 97 genes of interest (**Figure 7B**). The top ten genes
232 down- and upregulated (assessed by log₂ fold differences in expression) by knockdown of HIF-
233 2 α are summarized in **Figure 7C**, while the complete list of these 97 genes can be found in
234 **Supplementary Table S1**.

235

236 Gene set enrichment analysis (GSEA) on the RNA sequencing data described above
237 demonstrated that two out of the top five processes connected to disease were cancer and tumor
238 morphology (with 29 and 8 out of 97 molecules, respectively; **Figure 7D**). Deeper analysis of
239 tumor morphology showed that genes associated with invasion of tumor cells and size and
240 volume of tumor were particularly enriched, i.e. these associated genes linked to specific
241 disease categories are not due to random chance but are statistically significant ($p < 0.05$)
242 (**Figure 7E**). Consistent with *in vivo* data, we identified cellular movement as one of the top
243 molecular and cellular functions affected, with invasion as well as migration of tumor cells and
244 epithelial-to-mesenchymal transition as predicted downstream pathways (**Figure 7E**). GSEA
245 also revealed enrichment of genes associated with arrest in embryo growth (**Figure 7D-E**). We

246 conclude that the predicted cellular functions derived from our RNA sequencing experiment
247 overlap with *in vivo* data (cf. **Figures 3-6**). Top networks from the RNA sequencing data
248 showed enrichment of two signaling pathways, the ephrin receptor- and phosphatidylinositol
249 3-kinase (PI3K) signaling pathways (**Figure 7F** and **Supplementary Figure S5A**, with full list
250 of gene ontology enriched processes in **Supplementary Table S2**).

251

252 Dividing the hits from RNA sequencing data that overlap with genes enriched for migration of
253 tumor cells revealed a large subset of genes that encode for plasma membrane associated- or
254 are secreted proteins (**Supplementary Figure S5B**). Several of these overlapping genes were
255 among the 97 significantly differentially expressed (with cut-off $p < 0.005$), suggesting a close
256 regulatory relationship between HIF-2 α and migration at least during these time points of
257 development.

258

259 Given the effects we observed on embryonic development *in vivo*, we mapped potential
260 upstream regulators of arrest in embryo growth. As expected, most genes were transcription
261 factors, including *EPASI* itself (**Figure 7G**). Among the predicted upstream regulators of
262 arrested growth, genes associated with stem cells, BMP signaling and EMT were highly
263 enriched (**Table 1** and **Supplementary Table S3**).

264

265 Two other predicted genes upstream of arrested embryo growth were *CDX2* and *HNF1B*, also
266 among the 97 significantly (cut-off $p < 0.005$) differentially expressed in the RNA sequencing
267 data. Deeper analysis of these genes revealed autocrine signaling as well as an interconnected
268 regulation between the two (**Supplementary Figure S5C**). EMT related genes *ZEB2* and

269 *SNAIL* are negatively regulated by both of these genes (**Supplementary Figure S5C**). In
270 addition, *CDX2* was predicted to regulate *MYCN*, a transcription factor commonly amplified in
271 aggressive neuroblastoma (**Supplementary Figure S5C**). Of the significantly (cut-off
272 $p < 0.005$) differentially expressed genes, *CDX2* and *HNF1B* were predicted to be upstream
273 regulators of *EPAS1*. The majority of predicted *EPAS1* upstream regulators were transcription
274 factors, and we observed an enrichment for stem cell associated genes (**Supplementary Table**
275 **S4**).

276

277 *Trunk neural crest associated genes are enriched in neuroblastoma*

278 Neuroblastoma has long been recognized as derived from sympathetic neuroblasts of trunk
279 neural crest based on marker expression and tumor localization (De Preter et al., 2006; Hoehner
280 et al., 1996). However, recent studies from Adameyko and colleagues (Furlan et al., 2017;
281 Kastriti et al., 2019; Soldatov et al., 2019) have raised questions regarding the origin of
282 chromaffin cells as well as neuroblasts during embryonic development. While chromaffin cells
283 mainly derive from Schwann cell precursors (Furlan et al., 2017), sympathetic neuroblasts are
284 derived from sympathoadrenal precursor cells (Kastriti et al., 2019). Using a recently published
285 dataset of migratory trunk neural crest enriched genes (Murko et al., 2018) as well as established
286 neural crest and developmental markers, we examined connections between neuroblastoma and
287 trunk neural crest cells. We compared expression of early neural crest marker *TFAP2B* as well
288 as trunk neural crest markers *RASL11B*, *TAGLN3*, *NRCAM*, *AGPAT4*, *FMN2*, *HES5*, *HES6*
289 (Murko et al., 2018) and *HOXC9* (Frith et al., 2018) in cancer cell lines of different origins
290 (Cancer Cell Line Encyclopedia (CCLE) containing >600 cell lines; cancer types with $n \geq 4$ cell
291 lines were selected for further analysis (R2; <http://hgserver1.amc.nl>)) demonstrating enriched
292 expression for the majority of these genes in neuroblastoma cells as compared to other cancer

293 types (**Figure 8A** and **Supplementary Figure S6A-C**). Cranial neural crest marker *HOXA2*
294 was on the other hand not enriched in neuroblastoma as compared to other cancer types
295 (**Supplementary Figure S6D**). Neuroblastoma patient-derived xenograft (PDX) cells have
296 been established from mouse models of orthotopic implantation of patient-derived tumor pieces
297 (Braekeveldt et al., 2015; Persson et al., 2017). These PDX cells retain characteristics of their
298 respective patient tumor and metastasize to clinically relevant sites *in vivo*. Real-time
299 quantitative PCR analyses demonstrated significant enrichment of neural crest (*TFAP2B*,
300 *SOX10*) and trunk neural crest (*RASL11B*, *FMN2*, *TAGLN3*, *NRCAM*, *HES6*, *HES5*, *AGPAT4*)
301 gene expression in neuroblastoma PDX cells as compared to cells from renal cell carcinoma
302 (RCC-4 and 786-0) and liver cancer cell lines (Hep3b) (**Figure 8B-C** and **Supplementary**
303 **Figure S6E**).

304

305 **Discussion**

306 It has long been assumed that the childhood tumor form of neuroblastoma derives from
307 sympathoadrenal neuroblasts. These assumptions have been based on the expression of proteins
308 in neuroblastoma that are also expressed by embryonic sympathetic neurons during normal
309 development, as well as the location where these tumors arise (i.e. along the sympathetic
310 ganglia). HIF-2 α has been implicated in tumor growth and is expressed in cancer stem cells of
311 several tumors including neuroblastoma. However, little has been known about its expression
312 and function during normal development. Here, we show that the HIF-2 α protein is expressed
313 in trunk neural crest cells and sympathetic neuroblasts during normal embryogenesis in three
314 different species: human, mouse and avian and examine its function using the chick embryo as
315 a model amenable to experimental manipulation. Comparable data across human, mouse and
316 avian tissue suggest that cross-species interpretation of further results is valid.

317

318 Either knock-down or overexpression of HIF-2 α in premigratory chick trunk neural crest
319 affects several important functions. Not only do embryos with dysregulated HIF-2 α have
320 developmental delays compared to controls, but they also exhibit altered neural crest gene
321 expression profiles. Consistent with observed *in vivo* effects, RNA sequencing demonstrates a
322 global genome level change after loss of HIF-2 α , with upregulation of genes involved in
323 invasive behavior and growth arrest. Furthermore, we observed altered trunk neural crest
324 migratory patterns as well as enhanced proliferative capacity of trunk neural crest cells *in vivo*,
325 as well as in our RNA sequencing data.

326

327 Despite extensive proliferation of trunk neural crest cells with dysregulated HIF-2 α expression,

328 the embryos as a whole develop at a slower pace than their control counterparts. In general, cell
329 division of trunk neural crest cells is limited during their active migratory phase. We speculate
330 that the observed embryonic delays relative to increased trunk neural crest cell proliferation
331 may be the result of a skewed cell division to migration ratio, with increased proliferation
332 perhaps causing a failure in cell migration.

333

334 The capacity to self-renew is an important feature of stem-like cells. Our data suggest that
335 *EPASI* knockout cells exhibit enhanced self-renewal, in line with observations in
336 neuroblastoma cells with aberrant HIF-2 α expression which are more immature and neural
337 crest-like (Pietras et al., 2008). In addition, crestospheres formed by HIF-2 α dysregulated single
338 cells were larger, a sign of enhanced proliferative capacity in agreement with our EdU results.

339

340 The RNA sequencing data revealed enrichment of two signaling pathways, the ephrin receptor-
341 and PI3K pathways. This suggests that environmental cues may be influencing trunk neural
342 crest behavior. Of note, we have recently identified that PI3K-mTORC2 regulates HIF-2 α
343 expression and functions as a valid treatment target in neuroblastoma (Mohlin et al., 2015;
344 Mohlin, Hansson, et al., 2019). Genes associated with migration of tumor cells mainly encode
345 for plasma membrane and secreted proteins, including several members of the matrix
346 metalloproteinase (MMP) family. MMPs promote invasion and migration by degrading
347 components of the extracellular matrix and have been shown to be regulated by HIF-2 α in
348 several different tumor forms (Koh, Lemos, Liu, & Powis, 2011; Petrella, Lohi, & Brinckerhoff,
349 2005), further reinforcing a possible connection between HIF-2 α , trunk neural crest cells and
350 invasive behavior.

351

352 The stem cell gene *POU5F1*, more commonly known as Oct4, is driven by HIF-2 α in immature
353 cells during development (Covello et al., 2006). We found that Oct4 is predicted to be upstream
354 of arrested embryo growth, but also an upstream regulator of *EPASI* itself. One of the *EPASI*
355 target molecules connecting Oct4 and HIF-2 α is *CDX2*, which in turn is upstream of *EPASI* as
356 well as arrested embryo growth (**Supplementary Figure S5C**). *CDX2* is indeed one of the
357 major players involved in mediating the HIF-2 α driven effects on embryonic development and
358 considering that *CDX2* is an early trunk neural crest marker (Frith et al., 2018), a possible
359 explanation for delayed embryonic development might be halted trunk neural crest
360 commitment.

361

362 These findings contribute to understanding of a complex regulatory network involved in
363 mediating trunk neural crest development. We posit that the cancer associated protein HIF-2 α
364 may play a central role in embryonic growth, global gene expression, migration, proliferation
365 and stem cell features of neural crest cells within this network (**Figure 8D**). Moreover, our
366 results highlight the importance of careful regulation of HIF-2 α levels for maintenance of
367 normal embryonic growth and differentiation.

368

369 **Materials and Methods**

370 *Chick embryo tissue*

371 According to Swedish regulations (Jordbruksverkets föreskrift L150, §5) work on chick
372 embryos younger than embryonic day 13 do not require Institutional Animal Care and Use
373 Committee oversight.

374

375 *Human and mouse fetal tissue*

376 Human fetal tissue (ethical approval Dnr 6.1.8-2887/2017, Lund University, Sweden) was
377 obtained from elective abortions. Tissue samples were dissected in custom-made hibernation
378 medium (Life Technologies) and fixed in 4% formaldehyde overnight. Following a sucrose
379 gradient, embryos were embedded in gelatin for transverse sectioning at 12 μ m (ew5) or 7 μ m
380 (ew6) using a cryostat.

381

382 *Embryos and perturbations*

383 Chick embryos were acquired from commercially purchased fertilized eggs and incubated at
384 37.5°C until desired developmental Hamburger Hamilton (HH) stages were reached
385 (Hamburger & Hamilton, 1951). Optimal conditions for high transfection efficiency applying
386 one-sided electroporation *in ovo* were determined to 5 pulses of 30ms each at 22V. Ringer's
387 balanced salt solution (Solution-1: 144g NaCl, 4.5g CaCl \cdot 2H $_2$ O, 7.4g KCl, ddH $_2$ O to 500ml;
388 Solution-2: 4.35g Na $_2$ HPO $_4$ \cdot 7H $_2$ O, 0.4g KH $_2$ PO $_4$, ddH $_2$ O to 500ml (adjust final pH to 7.4))
389 containing 1% penicillin/streptomycin was used in all experiments. Morpholinos used were
390 from GeneTools with the following sequences; splice targeting EPAS1 oligo (5'-
391 GAAAGTGTGAGGGAACAAGTTACCT-3') and a corresponding 5'-mispair oligo (5'-
392 GAtAcTGTcAGGcAACAAcTTACCT-3'). Morpholinos were injected at a concentration of
393 1mM and co-electroporated with a GFP tagged empty control vector (1 ug/ul). RFP-tagged

394 *EPASI* overexpression construct and corresponding empty control vector were electroporated
395 at a concentration of 2.5 ug/ul. CRISPR constructs with gRNA non-targeting control (#99140,
396 Addgene) or gRNAs targeting *EPASI* (EPAS1.1.gRNA Top oligo – 5’
397 ggatgGCTCAGAACTGCTCctacc 3’, Bot oligo – 5’ aaacggtagGAGCAGTTCTGAGCc 3’;
398 EPAS1.2.gRNA Top oligo – 5’ ggatgAAGGCATCCATAATGCGCC 3’, Bot oligo – 5’
399 aaacGGCGCATTATGGATGCCTTc; 3’; EPAS1.3.gRNA Top oligo – 5’
400 ggatgAAATACATGGGTCTCACCC 3’, Bot oligo – 5’ aaacGGGTGAGACCCATGTATTTc
401 3’) were cloned into U6.3>gRNA.f+e (#99139, Addgene) and electroporated at a concentration
402 of 1.5 ug/ul, and accompanying Cas9 (#99138, Addgene) at 2 ug/ul (Gandhi, Haeussler, Razy-
403 Krajka, Christiaen, & Stolfi, 2017). Embryos were allowed to sit at room temperature for 8 –
404 10 hours in order to allow the Cas9 protein to fold before further incubation of the embryos at
405 37.5°C.

406
407 For harvesting of trunk neural crest cells for RNA extraction, embryos were incubated at 37.5°C
408 for 24 (morpholinos and overexpression vectors) or 36 (CRISPR/Cas9) hours post-
409 electroporation. Embryos were incubated for 24 to 48 hours post-electroporation before
410 dissecting whole embryos for fixation and embedding.

411 412 *Cloning*

413 To overexpress HIF-2 α , the gallus gallus *EPASI* coding sequence was amplified using the
414 following primers; Fwd:
415 5’AAACTCGAGGCCACCATGGACTACAAAGACGATGACGACAAGGCAGGTATGAC
416 AGCTGACAAGGAGAAG-3’, Rev 5’-AAAGCTAGCTCAGGTTGCCTGGTCCAG-3’ and
417 cloned into the pCI H2B-RFP vector (Addgene plasmid #92398). For CRISPR/Cas9 targeting,
418 oligos designed to target *EPASI* at three different locations (EPAS1.1, EPAS1.2 and EPAS1.3)

419 were annealed pairwise at a concentration of 100 μ M per oligo using T4 DNA Ligase Buffer in
420 dH₂O by heating to 95°C for 5 minutes. The annealed oligo reactions were cooled to room
421 temperature and diluted. The U6.3>gRNA.f+e (#99139, Addgene) vector was digested over
422 night with BsaI-HF enzyme (New England Biolabs) and gel extracted. gRNAs were cloned into
423 the digested U6.3>gRNA.f+e vector using T4 DNA Ligase (New England Biolabs) at room
424 temperature for 20 minutes. Successful inserts were identified by colony PCR using U6
425 sequencing primer and gRNA reverse oligo specific to each *EPASI* gRNA.

426

427 *Cell culture*

428 The human neuroblastoma cell line SK-N-BE(2)c (ATCC; Manassas, VA, US) and
429 hepatocellular carcinoma cell line Hep3b (ATCC; Manassas, VA, US) were cultured in MEM
430 while renal cell carcinoma RCC4 and 786-O cell lines were cultured in DMEM, supplemented
431 with 10% fetal bovine serum and 100 units penicillin and 10 μ g/mL streptomycin. As part of
432 our laboratory routines, all cells were maintained in culture for no more than 30 continuous
433 passages and regularly screened for mycoplasma. SK-N-BE(2)c cells were authenticated by
434 SNP profiling (Multiplexion, Germany).

435

436 *Neural tube dissection*

437 Neural tubes from respective axial levels were carefully dissected out from embryos at
438 designated somite stages. For cranial-derived cultures, the very anterior tip was excluded, and
439 the neural tube was dissected until the first somite level as previously described (Kerosuo, Nie,
440 Bajpai, & Bronner, 2015). For trunk-derived cultures, the neural tube was dissected between
441 somite 10-15 as previously described (Mohlin & Kerosuo, 2019; Mohlin, Kunttas, et al., 2019).
442 Pools of neural tubes from 4 - 6 embryos were used for each culture.

443

444 *Crestosphere cell culture*

445 Neural tube derived cells were cultured in NC medium (DMEM with 4.5g/L glucose (Corning),
446 7.5% chick embryo extract (MP Biomedicals; Santa Ana, CA, USA), 1X B27 (Life
447 Technologies; Carlsbad, CA, US), basic fibroblast growth factor (bFGF, 20 ng/ml) (Peprotech;
448 Stockholm, Sweden), insulin growth factor -I (IGF-I, 20 ng/ml) (Sigma Aldrich; Darmstadt,
449 Germany), retinoic acid (RA; 60nM for cranial and 180nM for trunk, respectively) (Sigma
450 Aldrich; Darmstadt, Germany), and 25 ng/ml BMP-4 (for trunk) (Peprotech; Stockholm,
451 Sweden)) in low-adherence T25 tissue culture flasks as described previously (Mohlin &
452 Kerosuo, 2019; Mohlin, Kunttas, et al., 2019).

453

454 *Self-renewal assay*

455 Chick embryos at developmental HH stage 10+ were injected and electroporated with
456 CRISPR/Cas9 constructs and allowed to develop at 37.5°C to reach HH stage 13/14.
457 Crestosphere cultures were established from embryos electroporated with control, EPAS1.1 or
458 EPAS1.2 constructs, respectively. Crestospheres were dissociated into single cells using
459 Accutase (Sigma Aldrich; incubation at 37 °C for 40 min with one minute of pipetting every
460 10 min), and individual cells were manually picked using a p10 pipette tip under the
461 microscope. Single cells were transferred to 96-well plates prepared with 100 µl of NC medium
462 supplemented with retinoic acid and BMP-4 (Mohlin, Kunttas, et al., 2019). The absolute
463 number of spheres formed in each well was quantified manually under the microscope. Five
464 wells were analyzed per crestosphere culture. Sphere diameter was manually measured using
465 the ImageJ software (spheres measured n=33 and n=27 for CTRL and EPAS1.2, respectively).

466

467 *EdU pulse chase labelling*

468 Proliferation was measured using the Click-iT™ EdU Cell Proliferation kit (Invitrogen
469 #C10337) according to the manufacturer's recommendations with optimizations from Warren
470 et al (Warren, Puskarczyk, & Chapman, 2009). Chick embryos at developmental HH stage 10+
471 were injected and electroporated with morpholino or overexpression constructs and allowed to
472 develop for additional 24 hours at 37.5°C. Eggs were then re-opened and EdU solution (500µM
473 in PBS-DEPC) was added. Eggs were re-sealed and incubated at 37.5°C for another 4 hours
474 before embryos were dissected in Ringer's solution and fixed in 4% paraformaldehyde
475 overnight. Embryos were washed in PBS-DEPC, H₂O and 3% BSA in PBS-DEPC before
476 permeabilization in 0.5% Triton-X. Embryos were hybridized in reaction cocktail (Click-iT
477 Reaction buffer, CuSO₄, Alexa Fluor 488 Azide and reaction buffer additive), washed and then
478 DAPI stained. Embryos were after another round of washing processed through a sucrose
479 gradient and embedded in gelatin.

480

481 *RNA sequencing*

482 Chick embryos of stage HH10+ were injected with EPAS1 targeting or corresponding 5'-
483 mispair morpholinos in the lumen of the neural tube and subsequently electroporated for
484 construct uptake. Following 24 hours of incubation at 37.5°C, embryos were removed from the
485 eggs in Ringer's solution. Neural tubes from the trunk axial level of individual embryos were
486 carefully dissected, removing surrounding mesodermal tissue, and transferred to Eppendorf
487 tubes (neural tube tissue from one embryo per Eppendorf) that were snap frozen. RNA was
488 extracted from each neural tube (5 samples per condition (EPAS1 and 5'-mispair, respectively))
489 using the RNAqueous Micro Kit (Ambion, #AM1931). Sequencing was performed using
490 NextSeq 500 (Illumina). Alignment of reads was performed using the HISAT2 software and

491 the reference genome was from the Ensemble database (Gallus gallus 5.0). Expression counts
492 were performed using the StringTie software and differentially expressed genes (DEG) analysis
493 was performed using DESeq2. To obtain a relevant working list out of the 1105 significantly
494 DEGs, we set a cut-off at $p < 0.005$ and removed all hits that were not annotated (NA), ending
495 up with 97 genes. Significance (p values) were DESeq2 derived (Love, Huber, & Anders,
496 2014). RNA sequencing data have been deposited in NCBI's Gene Expression Omnibus (Edgar,
497 Domrachev, & Lash, 2002) and are accessible through GEO Series accession number
498 GSE140319.

499

500 *Bioinformatics*

501 Gene Set Enrichment Analysis (GSEA) for gene ontology, network and functional analyses
502 were generated through the use of Panther database (analyses performed autumn 2018;
503 (<http://pantherdb.org/>) (Thomas et al., 2003) together with the Ingenuity Pathway Analysis
504 (IPA) software (Kramer, Green, Pollard, & Tugendreich, 2014) (QIAGEN Inc.,
505 <https://www.qiagenbioinformatics.com/products/ingenuity-pathway-analysis>). The use of the
506 two databases/software contributed to an added biological value in terms of knowledge. For a
507 hypothesis-free/exploratory analysis of the 97 DEGs, IPA was used (p-value calculations using
508 right-tailed Fisher Exact Test). However, IPA was mainly used for deeper exploration of the
509 data where the biological hypotheses generated for the project were further explored. Here, a
510 hypotheses-driven approach was taken where the following categories found from the IPA
511 analysis of the 97 DEGs were further investigated; “Cellular Movement”, within the
512 “Molecular and Cellular Function” result category, “Embryonic Development”, within the
513 category “Physiological System Development and Function”, and “Tumor Morphology”,
514 within the “Disease and Disorders” category. These three biological networks were further

515 investigated within the data set at hand. The investigation for the possible overlap and
516 connections between these networks in the context of the data were hence explored.

517

518 *Whole mount in situ hybridization of crestospheres*

519 For whole mount *in situ* hybridization, crestospheres were fixed in 4% PFA for 30 minutes at
520 RT and washed in DEPC-PBT. Samples were gradually dehydrated by bringing them to 100%
521 MeOH and kept at -20°C until use. *In situ* hybridization was performed as previously described
522 (Acloque, Wilkinson, & Nieto, 2008). Crestospheres were rehydrated back to 100% PBT,
523 treated with Proteinase K/PBT, washed in 2 mg/ml glycine/PBT and post-fixed in 4%
524 paraformaldehyde / 0.2% glutaraldehyde for 20 minutes. Crestospheres were then
525 prehybridized in hybridization buffer for 2 hours at 70°C and hybridized with Digoxigenin
526 (DIG)-labeled EPAS1 probe overnight at 70°C. Crestospheres were washed in Wash solution I
527 and II (50% formamide, 1% SDS [Sodium Dodecyl Sulfate] and 5X SSC [NaCl and Na citrate]
528 or 2X SSC, respectively), and blocked in 10% Sheep Serum for 2 hours followed by incubation
529 with an anti-DIG antibody (1:2000) (Roche) in TBST / 1% sheep serum overnight at 4°C. On
530 day 3, embryos were washed in TBST throughout the day and overnight. Crestospheres were
531 washed in Alkaline phosphatase buffer (NTMT; 100mM NaCl, 100mM Tris-Cl (pH 9.5),
532 50mM MgCl₂, 1%Tween-20) before visualizing the signal using 1-Step™ NBT/BCIP
533 Substrate Solution (ThermoFisher #34042). Stained crestospheres were fixed in 4% PFA for 20
534 minutes when they reached the desired state and dehydrated in MeOH to be stored at -20°C.
535 Embryos were embedded in blocks of gelatin for transverse sectioning at 20 µm using a
536 cryostat. Hybridization probe for avian *EPAS1* was prepared by using the following primers
537 (Forward 5'- CAAGGAGAAGAAGAGGAGCA -3'; Reverse 5'-
538 AAAGTGTGAGGAGGGCAAG -3') and chick embryo cDNA as template. The amplified

539 sequence was cloned into a pGEM-T Easy Vector before digestion and DIG RNA labeling
540 (Roche #11277073910).

541

542 *Cryosections*

543 Fixed embryos and crestospheres were incubated in a sucrose gradient (5% sucrose for 10
544 minutes and 15% sucrose for 10 minutes up to several hours) followed by incubation in 7.5%
545 gelatin over night at 37°C. Embedded samples were cryosectioned at 7, 10, 12 or 20 µm.

546

547 *Immunohistochemistry and immunofluorescence*

548 Immunohistochemistry on human (antigen retrieval by Target Retrieval Solution pH6.0
549 (DAKO #S1699)) and mouse fetal tissue was performed using Autostainer (Dako) and sections
550 were counterstained with hematoxylin. Detection of HIF-2 α by immunofluorescence was
551 performed by incubation of embryo sections in ice cold acetone followed by 0.3% Triton-X in
552 PBS. After washing in PBS, slides were blocked in DAKO serum-free ready-to-use block
553 (DAKO, #X0909) for 1 hour before incubation with primary antibody (in DAKO antibody
554 diluent with background reducing components (DAKO, #S3022)) overnight. Slides were
555 washed in PBS and incubated with rabbit linker (DAKO, #K8019) followed by secondary
556 antibody in 1% BSA/PBS. Detection of HNK1 and SOX9 by immunofluorescence was
557 performed by blocking (10% goat serum and 0.3% Triton-X in TBST) of embryo sections
558 followed by incubation with primary antibodies over night at +4°C. Slides were washed and
559 incubated with secondary antibodies and DAPI for nuclear staining for 1 hour at RT before
560 washing and mounting. Fluorescent images were acquired using an Olympus BX63
561 microscope, DP80 camera, and cellSens Dimension v 1.12 software (Olympus Cooperation).
562 Detailed information on antibodies can be found in Supplemental Table S5.

563

564 *RNA extraction and quantitative real-time PCR*

565 Total RNA was extracted using the RNAqueous Micro Kit (Ambion, #AM1931). Wild type
566 whole embryos were carefully mechanically dissociated before lysis, pooling 2 to 4 embryos
567 for each developmental stage. cDNA synthesis using random primers and qRT-PCR was
568 performed as previously described (Mohlin et al., 2015). Relative mRNA levels were
569 normalized to expression of two (avian; *18S*, *28S*) or three (human; *UBC*, *SDHA*, *YWHAZ*)
570 reference genes using the comparative Ct method (Vandesompele et al., 2002). Detailed
571 information of primer sequences can be found in Supplementary Table S6.

572

573 *Fractionation and western blot*

574 Cytoplasmic and nuclear extraction of proteins was performed using the NE-PER Nuclear and
575 Cytoplasmic Extraction Reagents (Thermo Scientific). Proteins were separated by SDS-PAGE
576 and transferred to HyBond-C-Extra nitrocellulose membranes. Detailed information on
577 antibodies can be found in Supplemental Table S5.

578

579 *Oxygen sensing*

580 Oxygen concentrations were measured through the trunk region of developing chick embryos
581 *ex ovo* using microsensors in a flow system of MQ water. Microprofiles were measured in 50
582 embryos in developmental stages HH10 to HH24. Embryos were removed from the egg using
583 filter paper as described in Mohlin and Kerosuo (Mohlin & Kerosuo, 2019), submerged in a
584 plate with constant flow of newly shaken MQ of room temperature, and immediately measured.
585 Oxygen microsensors were constructed and calibrated as described by Revsbech and Andersen
586 (Revsbech & Andersen, 1989), mounted on a micromanipulator. The microsensor was

587 manually probing the trunk region and data logged every second. Within the microprofile, ten
588 consecutive data points of the lowest oxygen concentrations were averaged and set as
589 representing the trunk neural tube. A two-point calibration was performed using the newly
590 shaken MQ (100% oxygen saturation) and by adding sodium dithionite to non-flowing MQ in
591 the plate after measurements (0% oxygen saturation). Salinity of the tissue was determined
592 using a conductivity meter (WTW 3110) and room temperature noted. The tissue is considered
593 a liquid, where full oxygen saturation at 5 ‰ salinity and 25°C corresponds to 250 $\mu\text{m/l}$, 160
594 mmHg or 21% atmospheric O_2 . Data was averaged for each HH stage including one
595 measurement of the previous and subsequent HH stages. Replicates vary from three to ten
596 biologically independent data points. Data is presented as percent of maximum saturation in the
597 solution of the specific temperature and salinity.

598

599 *Quantifications*

600 Embryonic development was quantified in two ways; by determining the HH stage of embryos
601 *in ovo* using head and tail morphology or by counting the number of somites of dissected
602 embryos *ex ovo*. The number of embryos (n) for each group is denoted in respective figure
603 legend. The fraction of proliferating EdU+ cells was determined by quantifying the number of
604 GFP+ proliferating cells as well as RFP+ construct targeted cells and divide the number of
605 double positive cells with the number of RFP+ cells. Only neural crest cells were included
606 (distinguished by the dotted line in figures).

607

608 *Statistical methods and data sets*

609 One-way ANOVA or two-sided student's unpaired *t* test was used for statistical analyses.
610 Publicly available dataset Cancer Cell Line Encyclopedia (CCLE) (R2: microarray analysis and
611 visualization platform (<http://r2.amc.nl>)) was used to analyze gene expression across cell lines

612 from different cancer types. For downstream analysis on the 97 DEGs where the software IPA
613 was used, the statistical tests considered were p-value calculations using right-tailed Fisher
614 Exact Test.

615

616 **Acknowledgments**

617 We would like to thank Erica Hutchins, Shashank Gandhi and Siv Beckman for skillful
618 technical assistance and Anni Glud and Ronnie N. Glud for providing microsensor technique
619 and expertise. This work was supported by the Swedish Cancer Society, the Swedish Childhood
620 Cancer Fund, the Craaford Foundation, Jeansson Foundations, Ollie and Elof Ericsson's
621 foundation, the Mary Bevé Foundation, Magnus Bergvall's foundation, the Thelma Zoéga
622 foundation for medical research, Hans von Kantzow's foundation, the Royal Physiographic
623 Society of Lund, the Gyllenstierna Krapperup's Foundation, and Gunnar Nilssons
624 Cancerstiftelse (to SM), DE027568 and R01HL14058 (to MEB). We thank Center for
625 Translational Genomics, Lund University and Clinical Genomics Lund, SciLifeLab for
626 providing sequencing service. Support by NBIS (National Bioinformatics Infrastructure
627 Sweden) is gratefully acknowledged.

628

629 **Author contributions**

630 SM, CUP, EF and EH performed experiments. SM, EH and MEB analyzed data. SM and JML
631 analyzed RNA sequencing data. EM and ZK provided materials. SM and MEB supervised the
632 study. SM wrote the original draft of the manuscript while all authors reviewed and edited the
633 manuscript.

634

635 **Competing interests**

636 The authors declare no competing interests.

637

638

639

640

641 **References**

- 642 Acloque, H., Wilkinson, D. G., & Nieto, M. A. (2008). In situ hybridization analysis of chick
643 embryos in whole-mount and tissue sections. *Methods Cell Biol*, 87, 169-185.
644 doi:10.1016/S0091-679X(08)00209-4
- 645 Ayer-Le Lievre, C. S., & Le Douarin, N. M. (1982). The early development of cranial sensory
646 ganglia and the potentialities of their component cells studied in quail-chick chimeras.
647 *Dev Biol*, 94(2), 291-310. doi:10.1016/0012-1606(82)90349-9
- 648 Bishop, T., Gallagher, D., Pascual, A., Lygate, C. A., de Bono, J. P., Nicholls, L. G., . . .
649 Ratcliffe, P. J. (2008). Abnormal sympathoadrenal development and systemic
650 hypotension in PHD3^{-/-} mice. *Mol Cell Biol*, 28(10), 3386-3400.
651 doi:10.1128/MCB.02041-07
- 652 Bittencourt, D. A., da Costa, M. C., Calloni, G. W., Alvarez-Silva, M., & Trentin, A. G. (2013).
653 Fibroblast growth factor 2 promotes the self-renewal of bipotent glial smooth muscle
654 neural crest progenitors. *Stem Cells Dev*, 22(8), 1241-1251. doi:10.1089/scd.2012.0585
- 655 Braekeveldt, N., Wigerup, C., Gisselsson, D., Mohlin, S., Merselius, M., Beckman, S., . . .
656 Bexell, D. (2015). Neuroblastoma patient-derived orthotopic xenografts retain
657 metastatic patterns and geno- and phenotypes of patient tumours. *Int J Cancer*, 136(5),
658 E252-261. doi:10.1002/ijc.29217
- 659 Bronner-Fraser, M., & Fraser, S. E. (1988). Cell lineage analysis reveals multipotency of some
660 avian neural crest cells. *Nature*, 335(6186), 161-164. doi:10.1038/335161a0
- 661 Covello, K. L., Kehler, J., Yu, H., Gordan, J. D., Arsham, A. M., Hu, C. J., . . . Keith, B. (2006).
662 HIF-2alpha regulates Oct-4: effects of hypoxia on stem cell function, embryonic
663 development, and tumor growth. *Genes Dev*, 20(5), 557-570. doi:10.1101/gad.1399906
- 664 De Preter, K., Vandesompele, J., Heimann, P., Yigit, N., Beckman, S., Schramm, A., . . .
665 Speleman, F. (2006). Human fetal neuroblast and neuroblastoma transcriptome analysis

- 666 confirms neuroblast origin and highlights neuroblastoma candidate genes. *Genome Biol*,
667 7(9), R84. doi:10.1186/gb-2006-7-9-r84
- 668 Edgar, R., Domrachev, M., & Lash, A. E. (2002). Gene Expression Omnibus: NCBI gene
669 expression and hybridization array data repository. *Nucleic Acids Res*, 30(1), 207-210.
670 doi:10.1093/nar/30.1.207
- 671 Frith, T. J., Granata, I., Wind, M., Stout, E., Thompson, O., Neumann, K., . . . Tsakiridis, A.
672 (2018). Human axial progenitors generate trunk neural crest cells in vitro. *Elife*, 7.
673 doi:10.7554/eLife.35786
- 674 Furlan, A., Dyachuk, V., Kastriti, M. E., Calvo-Enrique, L., Abdo, H., Hadjab, S., . . .
675 Adameyko, I. (2017). Multipotent peripheral glial cells generate neuroendocrine cells
676 of the adrenal medulla. *Science*, 357(6346). doi:10.1126/science.aal3753
- 677 Gandhi, S., Haeussler, M., Razy-Krajka, F., Christiaen, L., & Stolfi, A. (2017). Evaluation and
678 rational design of guide RNAs for efficient CRISPR/Cas9-mediated mutagenesis in
679 *Ciona*. *Dev Biol*, 425(1), 8-20. doi:10.1016/j.ydbio.2017.03.003
- 680 Hamburger, V., & Hamilton, H. L. (1951). A series of normal stages in the development of the
681 chick embryo. *J Morphol*, 88(1), 49-92.
- 682 Hoehner, J. C., Gestblom, C., Hedborg, F., Sandstedt, B., Olsen, L., & Pahlman, S. (1996). A
683 developmental model of neuroblastoma: differentiating stroma-poor tumors' progress
684 along an extra-adrenal chromaffin lineage. *Lab Invest*, 75(5), 659-675.
- 685 Holmquist-Mengelbier, L., Fredlund, E., Lofstedt, T., Noguera, R., Navarro, S., Nilsson, H., . .
686 . Pahlman, S. (2006). Recruitment of HIF-1alpha and HIF-2alpha to common target
687 genes is differentially regulated in neuroblastoma: HIF-2alpha promotes an aggressive
688 phenotype. *Cancer Cell*, 10(5), 413-423. doi:10.1016/j.ccr.2006.08.026
- 689 Kastriti, M. E., Kameneva, P., Kamenev, D., Dyachuk, V., Furlan, A., Hampl, M., . . .
690 Adameyko, I. (2019). Schwann Cell Precursors Generate the Majority of Chromaffin

- 691 Cells in Zuckerkandl Organ and Some Sympathetic Neurons in Paraganglia. *Front Mol*
692 *Neurosci*, 12, 6. doi:10.3389/fnmol.2019.00006
- 693 Kerosuo, L., Nie, S., Bajpai, R., & Bronner, M. E. (2015). Crestospheres: Long-Term
694 Maintenance of Multipotent, Premigratory Neural Crest Stem Cells. *Stem Cell Reports*,
695 5(4), 499-507. doi:10.1016/j.stemcr.2015.08.017
- 696 Khudyakov, J., & Bronner-Fraser, M. (2009). Comprehensive spatiotemporal analysis of early
697 chick neural crest network genes. *Dev Dyn*, 238(3), 716-723. doi:10.1002/dvdy.21881
- 698 Koh, M. Y., Lemos, R., Jr., Liu, X., & Powis, G. (2011). The hypoxia-associated factor switches
699 cells from HIF-1alpha- to HIF-2alpha-dependent signaling promoting stem cell
700 characteristics, aggressive tumor growth and invasion. *Cancer Res*, 71(11), 4015-4027.
701 doi:10.1158/0008-5472.CAN-10-4142
- 702 Kramer, A., Green, J., Pollard, J., Jr., & Tugendreich, S. (2014). Causal analysis approaches in
703 Ingenuity Pathway Analysis. *Bioinformatics*, 30(4), 523-530.
704 doi:10.1093/bioinformatics/btt703
- 705 Love, M. I., Huber, W., & Anders, S. (2014). Moderated estimation of fold change and
706 dispersion for RNA-seq data with DESeq2. *Genome Biol*, 15(12), 550.
707 doi:10.1186/s13059-014-0550-8
- 708 Maris, J. M. (2010). Recent advances in neuroblastoma. *N Engl J Med*, 362(23), 2202-2211.
709 doi:10.1056/NEJMra0804577
- 710 Mohlin, S., Hamidian, A., & Pahlman, S. (2013). HIF2A and IGF2 expression correlates in
711 human neuroblastoma cells and normal immature sympathetic neuroblasts. *Neoplasia*,
712 15(3), 328-334. doi:10.1593/neo.121706
- 713 Mohlin, S., Hamidian, A., von Stedingk, K., Bridges, E., Wigerup, C., Bexell, D., & Pahlman,
714 S. (2015). PI3K-mTORC2 but not PI3K-mTORC1 regulates transcription of

- 715 HIF2A/EPAS1 and vascularization in neuroblastoma. *Cancer Res*, 75(21), 4617-4628.
716 doi:10.1158/0008-5472.CAN-15-0708
- 717 Mohlin, S., Hansson, K., Radke, K., Martinez, S., Blanco-Apiricio, C., Garcia-Ruiz, C., . . .
718 Bexell, D. (2019). Anti-tumor effects of PIM/PI3K/mTOR triple kinase inhibitor IBL-
719 302 in neuroblastoma. *EMBO Mol Med*, 11(8), e10058.
720 doi:10.15252/emmm.201810058
- 721 Mohlin, S., & Kerosuo, L. (2019). In Vitro Maintenance of Multipotent Neural Crest Stem Cells
722 as Crestospheres. *Methods Mol Biol*, 2002, 1-11. doi:10.1007/7651_2018_180
- 723 Mohlin, S., Kunttas, E., Persson, C. U., Abdel-Haq, R., Castillo, A., Murko, C., . . . Kerosuo,
724 L. (2019). Maintaining multipotent trunk neural crest stem cells as self-renewing
725 crestospheres. *Dev Biol*, 447(2), 137-146. doi:10.1016/j.ydbio.2019.01.010
- 726 Murko, C., Vieceli, F. M., & Bronner, M. (2018). Transcriptome dataset of trunk neural crest
727 cells migrating along the ventral pathway of chick embryos. *Data Brief*, 21, 2547-2553.
728 doi:10.1016/j.dib.2018.11.109
- 729 Persson, C. U., von Stedingk, K., Bexell, D., Merselius, M., Braekeveldt, N., Gisselsson, D., .
730 . . Wigerup, C. (2017). Neuroblastoma patient-derived xenograft cells cultured in stem-
731 cell promoting medium retain tumorigenic and metastatic capacities but differentiate in
732 serum. *Sci Rep*, 7(1), 10274. doi:10.1038/s41598-017-09662-8
- 733 Petrella, B. L., Lohi, J., & Brinckerhoff, C. E. (2005). Identification of membrane type-1 matrix
734 metalloproteinase as a target of hypoxia-inducible factor-2 alpha in von Hippel-Lindau
735 renal cell carcinoma. *Oncogene*, 24(6), 1043-1052. doi:10.1038/sj.onc.1208305
- 736 Pietras, A., Gisselsson, D., Ora, I., Noguera, R., Beckman, S., Navarro, S., & Pahlman, S.
737 (2008). High levels of HIF-2alpha highlight an immature neural crest-like
738 neuroblastoma cell cohort located in a perivascular niche. *J Pathol*, 214(4), 482-488.
739 doi:10.1002/path.2304

- 740 Pietras, A., Hansford, L. M., Johnsson, A. S., Bridges, E., Sjolund, J., Gisselsson, D., . . .
741 Pahlman, S. (2009). HIF-2alpha maintains an undifferentiated state in neural crest-like
742 human neuroblastoma tumor-initiating cells. *Proc Natl Acad Sci U S A*, *106*(39), 16805-
743 16810. doi:10.1073/pnas.0904606106
- 744 Revsbech, P., & Andersen, G. (1989). Diurnal variation in peak expiratory flow rate among
745 grain elevator workers. *Br J Ind Med*, *46*(8), 566-569. doi:10.1136/oem.46.8.566
- 746 Soldatov, R., Kaucka, M., Kastriti, M. E., Petersen, J., Chontorotzea, T., Englmaier, L., . . .
747 Adameyko, I. (2019). Spatiotemporal structure of cell fate decisions in murine neural
748 crest. *Science*, *364*(6444). doi:10.1126/science.aas9536
- 749 Thomas, P. D., Campbell, M. J., Kejariwal, A., Mi, H., Karlak, B., Daverman, R., . . .
750 Narechania, A. (2003). PANTHER: a library of protein families and subfamilies
751 indexed by function. *Genome Res*, *13*(9), 2129-2141. doi:10.1101/gr.772403
- 752 Tian, H., Hammer, R. E., Matsumoto, A. M., Russell, D. W., & McKnight, S. L. (1998). The
753 hypoxia-responsive transcription factor EPAS1 is essential for catecholamine
754 homeostasis and protection against heart failure during embryonic development. *Genes
755 Dev*, *12*(21), 3320-3324. doi:10.1101/gad.12.21.3320
- 756 Vandesompele, J., De Preter, K., Pattyn, F., Poppe, B., Van Roy, N., De Paepe, A., & Speleman,
757 F. (2002). Accurate normalization of real-time quantitative RT-PCR data by geometric
758 averaging of multiple internal control genes. *Genome Biol*, *3*(7), RESEARCH0034.
759 doi:10.1186/gb-2002-3-7-research0034
- 760 Vega-Lopez, G. A., Cerrizuela, S., Tribulo, C., & Aybar, M. J. (2018). Neurocristopathies: New
761 insights 150 years after the neural crest discovery. *Dev Biol*, *444 Suppl 1*, S110-S143.
762 doi:10.1016/j.ydbio.2018.05.013
- 763 Warren, M., Puskarczyk, K., & Chapman, S. C. (2009). Chick embryo proliferation studies
764 using EdU labeling. *Dev Dyn*, *238*(4), 944-949. doi:10.1002/dvdy.21895

765

766

767

768 **Figure Legends**

769

770 **Fig. 1.** *HIF-2 α* is expressed in trunk neural crest cells. **A.** Western blot of fractionated wild
771 type HH18 chick embryos show HIF-2 α protein expression in cytoplasmic and nuclear
772 compartments (cf. panel **C-F**). Blot shown is a representative of multiple experiments. SDHA
773 was used as loading control. **B.** Relative mRNA expression over developmental time (HH4 to
774 HH27) in whole wild type chick embryos. *EPAS1* expression was measured using qRT-PCR
775 and is presented as mean of n=2 biological replicates. Error bars represent SEM. **C-D.**
776 Immunostaining of HIF-2 α in sections from trunk axial level of wild type chick embryos at
777 premigratory HH11 (**C**) and HH13 (**D**) stages. Arrows denote scattered HIF-2 α positive cells
778 within the dorsal neural tube. **E.** Immunostaining of HIF-2 α in sections from trunk axial level
779 of wild type chick embryos at migratory HH18 stage. Arrows denote ventrally migrating HIF-
780 2 α positive cells. **F.** A different section from embryo in (**E**) with magnification (dashed square).
781 **G.** Oxygen saturation (%) in the trunk of chick embryos during development measured *ex ovo*
782 using microsensor technique. Error bars represent SEM.

783

784 **Fig. 2.** *HIF-2 α* is expressed in human and mouse trunk neural crest cells. **A.**
785 Immunohistochemical staining of HIF-2 α in sections from a mouse embryo at embryonic day
786 E12.5. **B.** Immunohistochemical staining of TH in adjacent section to (**A**) to locate sympathetic
787 ganglia. **A-B.** Asterisk in left panels locate HIF-2 α ⁺ and TH⁺ cells within sympathetic ganglia.
788 Asterisk also indicate magnified area in middle panels and dashed square indicates
789 magnification area in right panels. **C.** Immunohistochemical staining of HIF-2 α in sections
790 from trunk axial level of a human embryo at embryonic week ew5. Arrowhead represents
791 magnification in upper right panel. Asterisk represents magnification in lower left panel and
792 dashed square represent magnified area in lower right panel. (**A-C**) Sections are counterstained

793 with hematoxylin to visualize tissue structure and nuclei. **D-E.** Immunostaining of HIF-2 α in
794 sections from trunk axial level of human embryos at embryonic week ew5 (**D**) and embryonic
795 week ew6 (**E**). Arrow denotes HIF-2 α positive migrating cells. ew, embryonic week; NC,
796 neural crest. DAPI was used to stain nuclei.

797

798 **Fig. 3. Knockdown of HIF-2 α delays embryogenesis.** **A.** Hamburger Hamilton (HH) staging of
799 embryos 36 hours post-electroporation with a non-targeting (CTRL) gRNA compared to three
800 different gRNAs targeting *EPAS1* (EPAS1.1, EPAS1.2, EPAS1.3) by head- and tail
801 morphology. Number of embryos analyzed were n=14 (CTRL), n=10 (EPAS1.1), n=14
802 (EPAS1.2) and n=14 (EPAS1.3). Statistical significance was determined by one-way ANOVA
803 comparing non-targeting CTRL with each individual *EPAS1* gRNA. **B.** Hamburger Hamilton
804 (HH) staging of embryos 44 hours post-electroporation with 5'-mispair or *EPAS1* targeting
805 morpholinos by head- and tail morphology. Number of embryos analyzed were n=20 (5'-
806 mispair), n=16 (EPAS1). Statistical significance was determined by one-way ANOVA. **C.**
807 Determination of embryonic age by number of somites 36 hours post-electroporation. Number
808 of embryos analyzed were n=8 (CTRL), n=13 (EPAS1.1) and n=14 (EPAS1.3). Statistical
809 significance was determined by one-way ANOVA comparing non-targeting CTRL with each
810 individual *EPAS1* gRNA. **D.** Determination of embryonic age by number of somites 44 hours
811 post-electroporation. Number of embryos analyzed were n=17 (5'-mispair), n=15 (EPAS1).
812 Statistical significance was determined by one-way ANOVA. **E-F.** Relative mRNA expression
813 of /trunk/ neural crest (**E**) and cranial neural crest (**F**) associated genes in trunk neural crest
814 cells derived from embryos electroporated with 5'-mispair or *EPAS1* morpholinos, measured
815 by qRT-PCR 24 hours post-electroporation. **G-H.** Relative mRNA expression of trunk neural
816 crest (**G**) and cranial neural crest (**H**) associated genes in trunk neural crest cells derived from
817 embryos electroporated with non-targeting CTRL or three *EPAS1* gRNAs, measured by qRT-

818 PCR 24 hours post-electroporation. **E-H.** Data presented as mean of n=2 biologically
819 independent repeats, error bars denote SEM. Statistical significance was determined by two-
820 sided student's t-test (**E-H**), comparing non-targeting CTRL with each individual *EPAS1*
821 gRNA in **G-H**.

822

823

824 **Fig. 4.** *Knockdown of HIF-2 α affects migration of trunk neural crest cells. A-D.*
825 Immunostaining of HNK1 (red) marking migrating crest cells in one-sided electroporated
826 embryos (right side). Electroporated cells (non-targeting CTRL gRNA (**A**), gRNA #2 targeting
827 *EPAS1* (EPAS1.2; **B**), 5'-mispair morpholino (**C**) or *EPAS1* morpholino (**D**)) are seen in green.
828 DAPI was used to counterstain nuclei. Embryo sections from trunk axial level are from 48 hours
829 (**A-B**) or 44 hours (**C-D**) post-electroporation.

830

831 **Fig. 5.** *Controlled expression of HIF-2 α is required to maintain embryonic homeostasis. A.*
832 Hamburger Hamilton (HH) staging of embryos 24 hours post-electroporation with a control
833 (pCI-CTRL) or *EPAS1* overexpression construct (pCI-EPAS1), determined by head- and tail
834 morphology. Number of embryos analyzed were n=16 (CTRL), n=20 (EPAS1). Statistical
835 significance was determined by one-way ANOVA. **B.** Immunostaining of HNK1 (green)
836 marking migrating crest cells in one-sided electroporated embryos (right side). Electroporated
837 cells (CTRL or EPAS1) are seen in red. DAPI was used to counterstain nuclei. Embryo sections
838 from trunk axial level are taken 48 hours post- electroporation. **C.** Relative mRNA expression
839 of /trunk/ neural crest and cranial neural crest genes in trunk neural crest cells derived from
840 embryos electroporated with CTRL or EPAS1 vectors, measured by qRT-PCR 24 hours post-
841 electroporation. Data presented as mean of n=2 biologically independent repeats, error bars
842 denote SEM. Statistical significance was determined by two-sided student's t-test.

843

844 **Fig. 6.** *Knockdown of HIF-2 α affects proliferation and stemness of trunk neural crest cells. A-*

845 **D.** Embryo sections from trunk axial level after real-time EdU labeling. Proliferating EdU⁺ cells

846 are seen in green and electroporated cells (5'-mispair and *EPAS1* morpholinos (**A**); pCI-CTRL

847 and pCI-EPAS1 (**C**)) are seen in red. DAPI was used to counterstain nuclei. Quantification of

848 proliferating cells was performed by manual counting of RFP⁺ only as well as double positive

849 cells. Only construct targeted trunk neural crest cells (above dotted line) were included. Number

850 of cells analyzed were n=82 (5'-mispair morpholino) and n=303 (*EPAS1* morpholino) (**B**);

851 n=211 (pCI-CTRL) and n=139 (pCI-EPAS1) (**D**). **E.** Relative mRNA expression of *EPAS1* in

852 wild type HH10 embryos (blue bar) and crestosphere cells established from the cranial axial

853 level (green bar) or trunk axial level (yellow bar) measured by qRT-PCR. Expression is

854 presented as mean of n=4 (cranial) or n=3 (trunk) biological replicates and error bars represent

855 SEM. Expression difference between cranial and trunk crestospheres, p=0.056, as determined

856 by two-sided student's t test. Expression in wild type HH10 embryos is presented as mean of

857 n=3 technical replicates. **F.** *In situ* detection of *EPAS1* mRNA in trunk derived crestospheres.

858 **G.** Primary sphere assay, i.e. quantification of self-renewal from crestospheres established from

859 dissociated trunk neural tubes of HH13+/14- embryos previously electroporated *in ovo* at

860 HH10⁺/HH11 with non-targeting gRNA (CTRL) or gRNA targeting *EPAS1* (*EPAS1.1*). One

861 cell/well (n=10 wells per group) were seeded at T= 0 days. Number of spheres were manually

862 counted in each well after T= 1 week. Statistical significance was determined by one-way

863 ANOVA. **H.** Quantification of self-renewal (as described in **G.**) and sphere size from

864 crestospheres established from dissociated trunk neural tubes of HH13+/14- embryos

865 electroporated with non-targeting gRNA (CTRL) or gRNA targeting *EPAS1* (*EPAS1.2*).

866 Sphere size by manual measurements converted to factual unit (μ m). Statistical significance

867 was determined by one-way ANOVA.

868

869 **Fig. 7.** *Gene set enrichment analysis identifies HIF-2 α downstream affected processes. A-B.*

870 Hierarchical clustering of significantly Differentially Expressed Genes (DEGs;cut-off p<0.005)

871 identified from RNA sequencing comparing 5'-mispair and *EPAS1* morpholino samples. **C.**

872 List of the top ten upregulated and top ten downregulated genes from the RNA sequencing data.

873 **D.** Hypothesis-free/exploratory analysis of the 97 DEGs using IPA (Fishers Exact Test for the

874 range of p-value calculation) revealed a series of top five hits (p<0.05) in the respective

875 categories “Disease and Disorders”, “Molecular and Cellular Functions” and “Physiological

876 System Development and Function” downstream processes. **E.** Deeper analysis of processes

877 identified in **(D)**. **F.** Selected list of enriched cellular processes from Panther analyses.

878 Complete list can be found in **Supplemental Table S2**. **G.** Deeper analysis of potential

879 upstream regulators of the “arrest in embryo growth” process identified in **E**. The shape of

880 molecules and their meaning, i.e. correspondence to protein family etc., is found here:

881 <http://qiagen.force.com/KnowledgeBase/KnowledgeIPAPage?id=kA41i000000L5rTCAS>. As

882 an example, the diamond shaped molecules correspond to enzymes, oval standing shapes

883 should be read as transmembrane receptors and lying oval shapes are transcription regulators.

884 Green nodes indicate down-regulated molecules. The intensity of the color reveals the strength

885 of the expression i.e. the stronger the color the more significant.

886

887 **Fig. 8.** *Trunk neural crest associated genes are enriched in neuroblastoma. A.* Trunk neural

888 crest (*RASL11B*, *TAGLN3* and *NRCAM*) gene expression in cancer types of different tissue

889 origins. Data from the Cancer Cell Line Encyclopedia (CCLE) dataset, tissue origin with

890 samples n>3 were chosen for further analysis. Number in brackets represents the number of cell

891 lines from each tissue origin. Arrows highlight neuroblastoma. **B-C.** Relative mRNA

892 expression of neural crest (*TFAP2B*, **(B)**) and trunk neural crest (*RASL11B*, *FMN2*, *TAGLN3*

893 and *NRCAM* (**C**) genes measured by qRT-PCR. Expression in LU-NB-3 neuroblastoma (NB)
894 patient-derived xenograft cells were compared to liver cancer (Li) Hep3B and clear cell renal
895 cell carcinoma (ccRCC) RCC-4 and 786-0 cell lines. Data are presented as mean of n=3
896 biologically independent replicates and error bars represent SEM. Statistical significance
897 comparing Hep3B, RCC-4 or 786-0 individually to LU-NB-3 was tested using two-sided
898 students *t test*. **D.** Schematic summary of developmental effects following dysregulated HIF-
899 2α expression levels in trunk neural crest cells.

900

901 **Table 1.** Selected genes identified as potential upstream regulators of arrested embryo growth.
902 Genes associated with stem cells (**A**), BMP signaling (**B**) and EMT (**C**) were particularly
903 enriched.

904

905 **Supplemental Fig. S1.** *Specificity control of antibodies.* **A.** Sections of HH13 wild type embryo
906 immunostained with DAPI for visualization of nuclei and secondary antibody only (donkey
907 anti-rabbit Alexa Fluor-546). **B.** Immunohistochemical staining for HIF- 2α in sections of SK-
908 N-BE(2)c neuroblastoma cells cultured at normoxia (21% O₂) or hypoxia (1% O₂). HIF- 2α
909 positive cells are as expected detected at hypoxia and demonstrate nuclear and cytoplasmic
910 expression.

911

912 **Supplemental Fig. S2.** *Electroporation of knockdown constructs is efficient.* **A-B.** Relative
913 mRNA expression of *EGFP* in embryos electroporated with morpholinos (cf. **Figure 3E-F**)
914 (**A**) or CRISPR constructs (cf. **Figure 3G-H**) (**B**) measured by qRT-PCR. Expression of *EGFP*
915 in electroporated embryos was compared to expression in wild type HH18 embryos. **C-D.**
916 Neural crest (**C**) and early or late/migratory neural crest (**D**) genes in trunk neural crest cells
917 derived from embryos electroporated with non-targeting (CTRL) or three *EPAS1* gRNAs,

918 measured by qRT-PCR 24 hours post-electroporation. Data are presented as mean of n=2
919 biologically independent replicates and error bars represent SEM. Statistical significance
920 comparing each individual *EPAS1* targeting gRNA to control (CTRL), respectively, was
921 determined by two-sided student's t-test.

922

923 **Supplemental Fig. S3.** *SOX9* expression is not affected by *HIF-2 α* knockdown. **A-C.**

924 Immunostaining of SOX9 (red) in one-sided electroporated embryos (right side).

925 Electroporated cells (non-targeting gRNA (CTRL), **(A)**) or gRNA #1 (EPAS1.1, **(B)**) and #3

926 (EPAS1.3, **(C)**) targeting EPAS1) are seen in green. DAPI was used to counterstain nuclei.

927 Embryo sections from trunk axial level are from 48 hours post-electroporation.

928

929 **Supplemental Fig. S4.** *Electroporation of overexpression constructs is efficient* **A.** Relative

930 mRNA expression of neural crest associated genes in trunk neural crest cells derived from

931 embryos electroporated with pCI-CTRL or pCI-EPAS1 vectors, measured by qRT-PCR 24

932 hours post-electroporation. Data presented as mean of n=2 biologically independent repeats,

933 error bars denote SEM. Statistical significance was determined by two-sided student's t-test. **B.**

934 Relative mRNA expression of *EPAS1* in embryos electroporated with pCI-CTRL or pCI-

935 EPAS1 for overexpression of *HIF-2 α* (cf. **Figure 5**). Data are presented as mean of n=2

936 biologically independent replicates and error bars represent SEM.

937

938 **Supplemental Fig. S5.** *Gene set enrichment analysis identifies key molecules.* **A.** Top network

939 composed by analyzing significantly Differentially Expressed Genes from RNA sequencing

940 data. **B.** Deeper analysis of overlap of genes involved in downstream process "migration of

941 tumor cells" and genes from RNA sequencing data. **A-B.** The shape of molecules and their

942 meaning, i.e. correspondence to protein family etc., is found here:

943 <http://qiagen.force.com/KnowledgeBase/KnowledgeIPAPage?id=kA41i000000L5rTCAS>. As
944 an example, the diamond shaped molecules correspond to enzymes, oval standing shapes
945 should be read as transmembrane receptors and lying oval shapes are transcription regulators.
946 Green nodes indicate down-regulated molecules. The intensity of the color reveals the strength
947 of the expression i.e. the stronger the color the more significant. The dashed lines indicate an
948 indirect interaction between molecules in the network whereas solid lines are direct interactions.
949 The solid arrow explains the direction of the indicated interaction. A line, solid or dashed,
950 without an arrowhead indicate an RNA-RNA interaction. **C.** Schematic of the gene regulatory
951 network including *EPASI* and downstream *CDX2* and *HNF1B* coupled to arrested embryo
952 growth.

953
954 **Supplemental Fig. S6.** *Trunk neural crest associated genes are enriched in neuroblastoma.* **A-**
955 **D.** Neural crest (*TFAP2B* (**A**)), trunk neural crest (*AGPAT4*, *FMN2*, *HES6*, *HES5* and *HOXC9*
956 (**B-C**)) and cranial neural crest (*HOXA2* (**D**)) gene expression in cancer types of different tissue
957 origins. Data from the Cancer Cell Line Encyclopedia (CCLE) dataset, tissue origin with
958 samples n>3 were chosen for further analysis. Arrows highlight neuroblastoma. **E.** Relative
959 mRNA expression of neural crest (*SOX10*) and trunk neural crest (*HES6*, *AGPAT4*, *HES5*)
960 genes measured by qRT-PCR. Expression in LU-NB-3 neuroblastoma (NB) patient-derived
961 xenograft cells were compared to liver cancer (Li) Hep3B and clear cell renal cell carcinoma
962 (ccRCC) RCC-4 and 786-0 cell lines. Data are presented as mean of n=3 biologically
963 independent replicates and error bars represent SEM. Statistical significance comparing Hep3B,
964 RCC-4 or 786-0 to LU-NB-3, respectively, was tested using two-sided students *t test*.

965
966 **Supplemental Table S1.** Full list of the 97 significantly ($p < 0.005$) DEGs between 5'-mispair
967 and *EPASI* morpholino samples identified by RNA sequencing. Relates to **Fig. 7A-B**.

968

969 **Supplemental Table S2.** Full list of processes identified by PANTHER analysis. Relates to

970 **Fig. 7F.**

971

972 **Supplemental Table S3.** Full list of genes identified as potential upstream regulators of “arrest

973 in embryo growth”. Relates to **Table 1.**

974

975 **Supplemental Table S4.** Full list of genes identified as potential upstream regulators of HIF-

976 2α from RNA sequencing data. Target molecules are among the 97 significantly ($p < 0.005$)

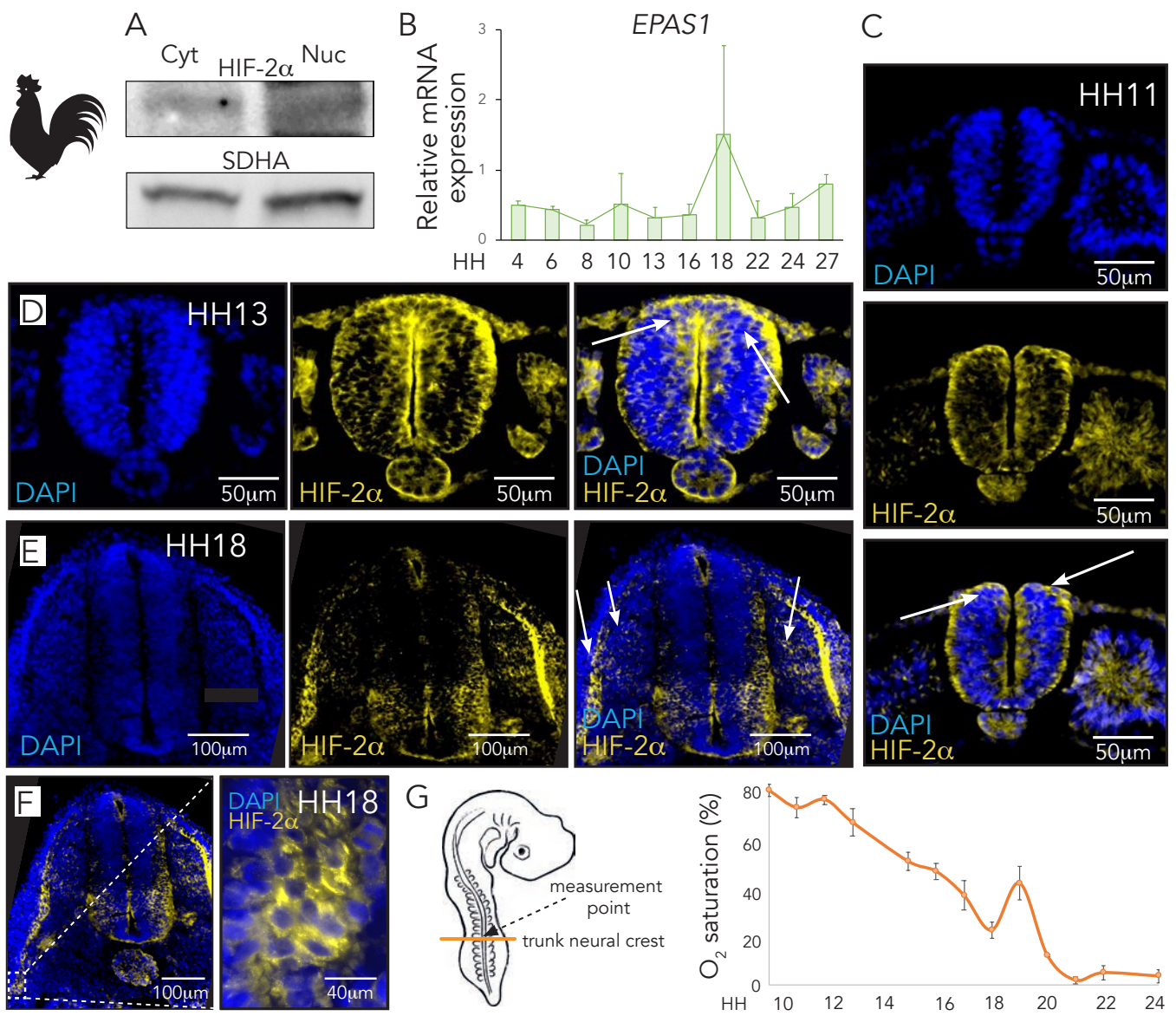
977 DEGs between 5'-mispair and *EPAS1* morpholino samples identified by RNA sequencing.

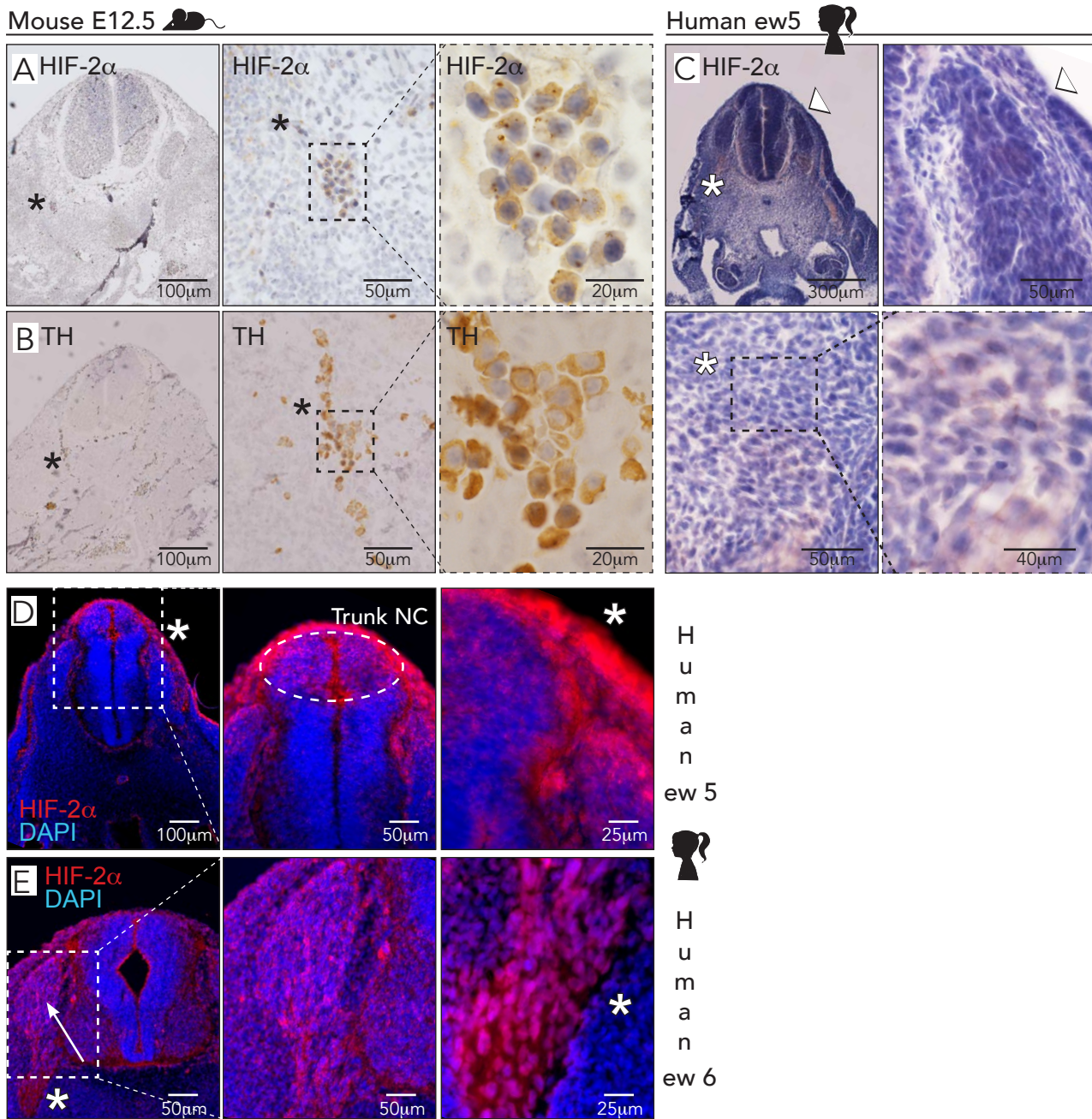
978

979 **Supplemental Table S5.** Details of antibodies.

980

981 **Supplemental Table S6.** List of primer sequences used for qRT-PCR analyses.





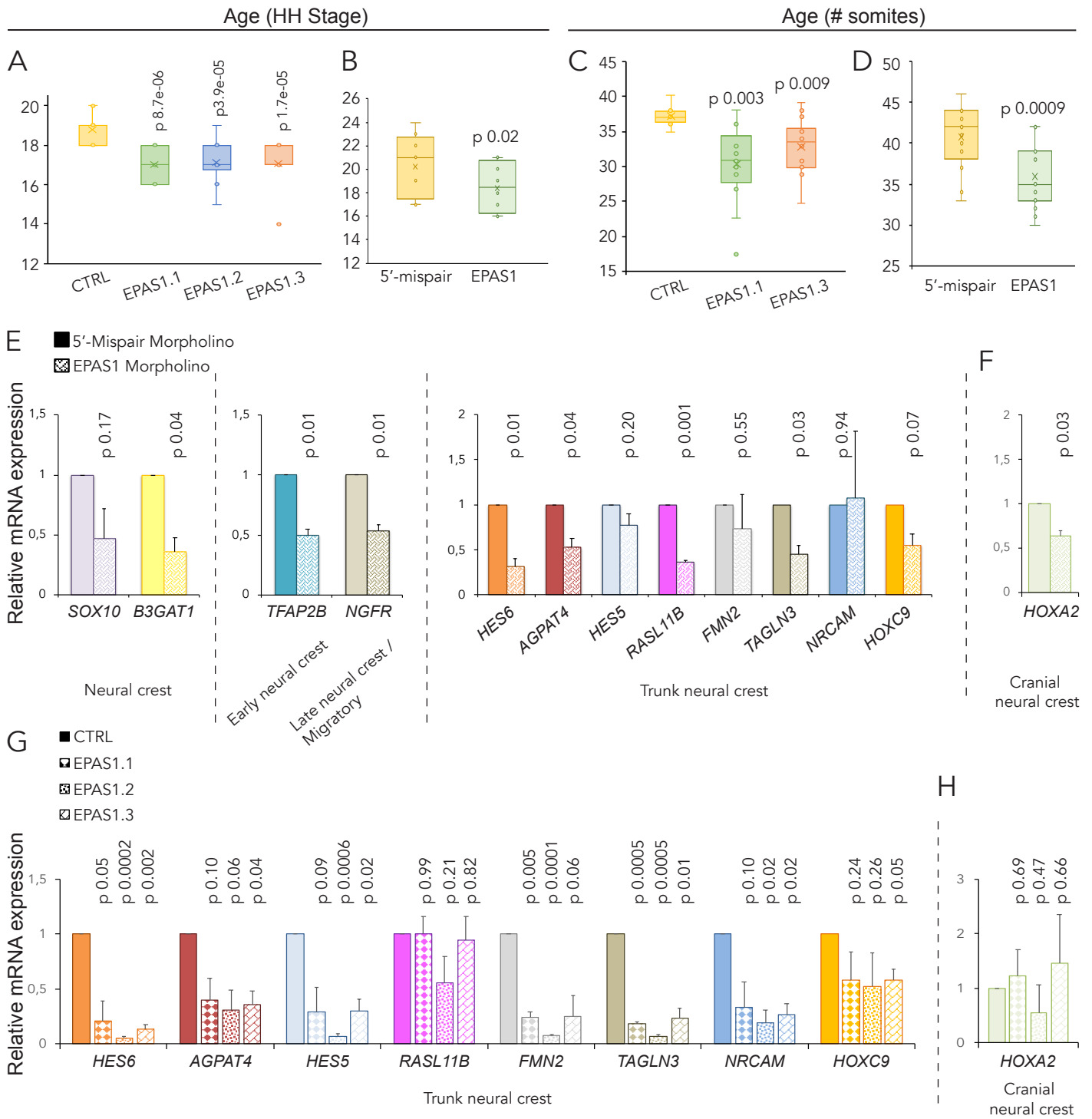
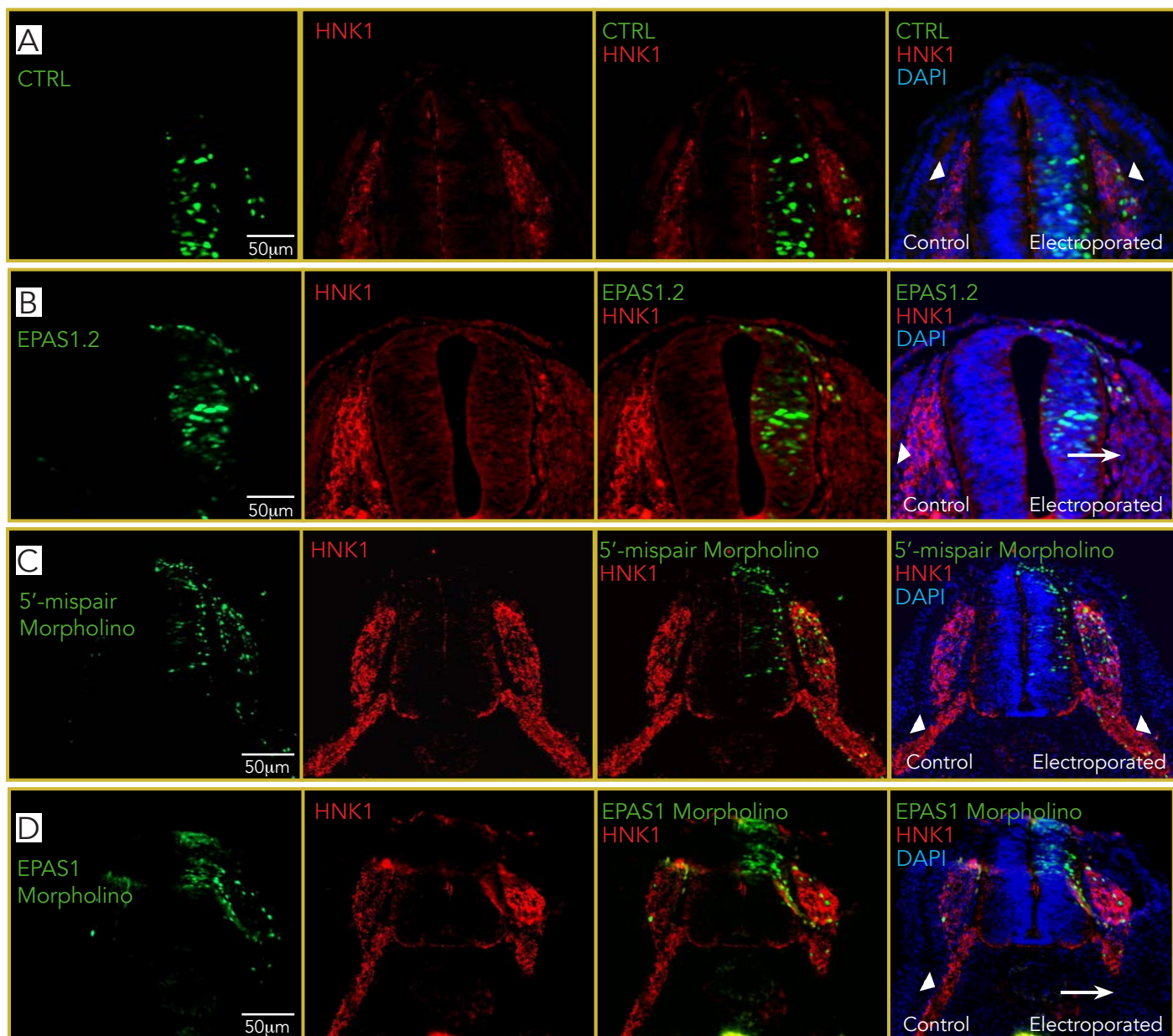
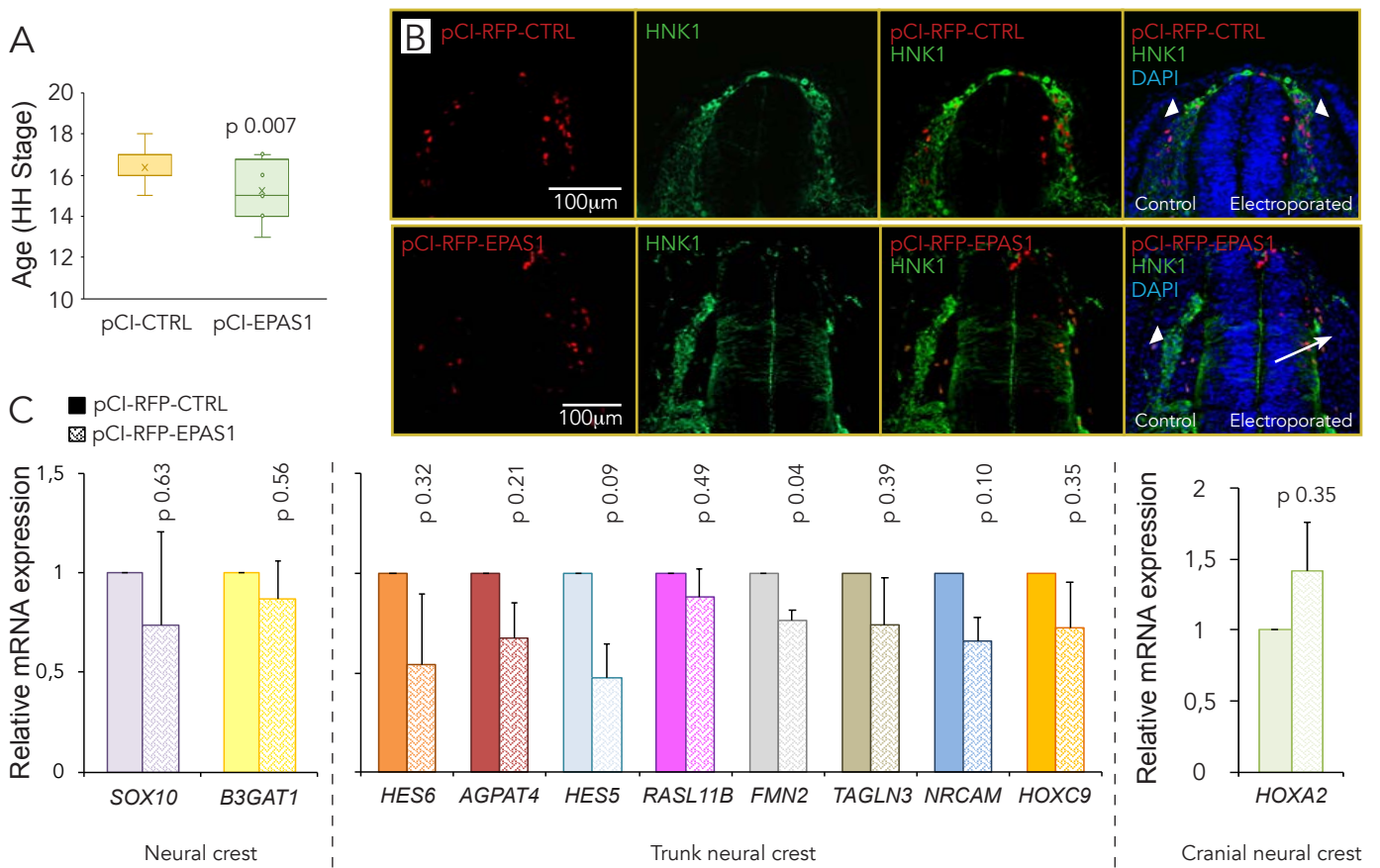
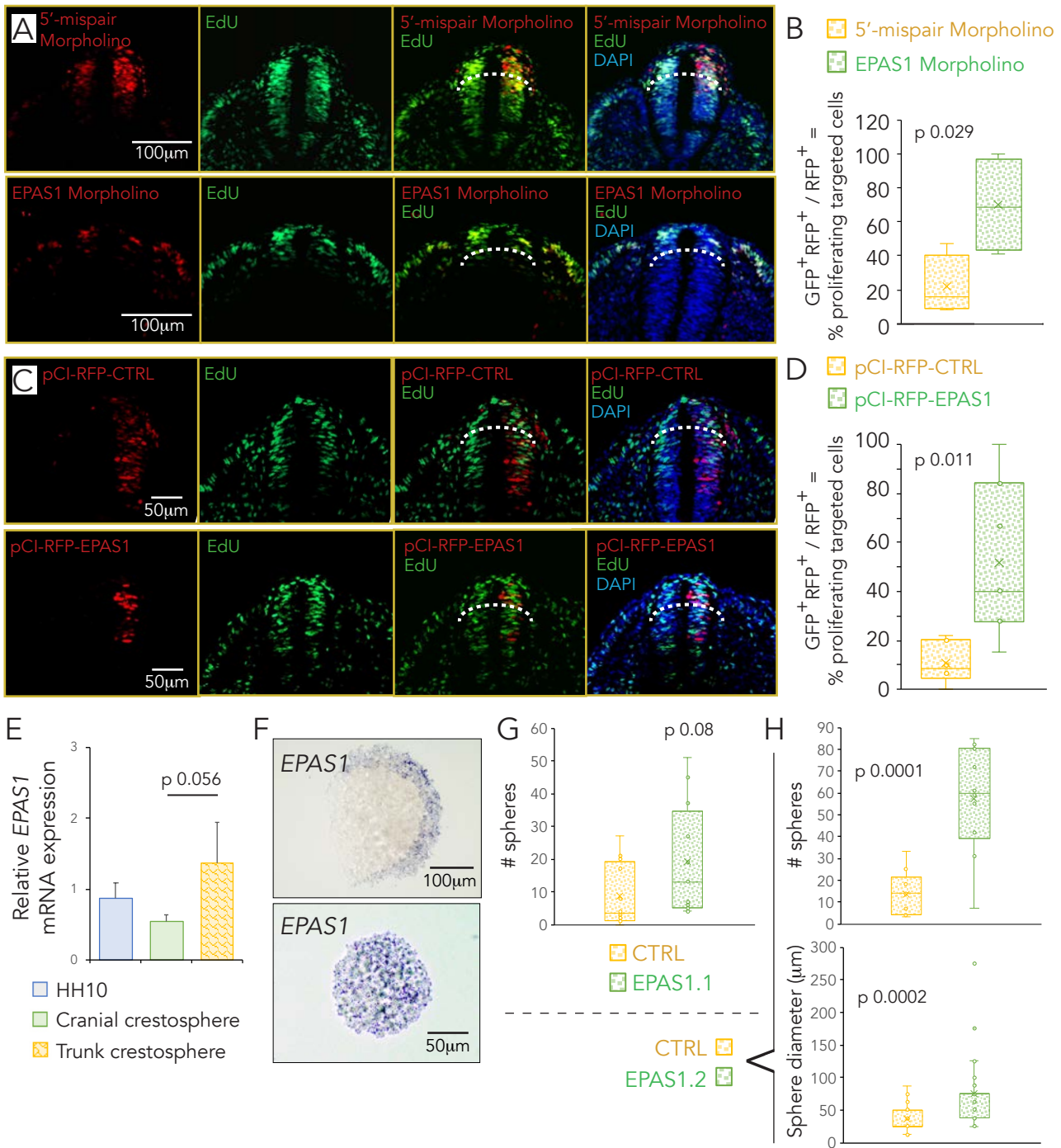
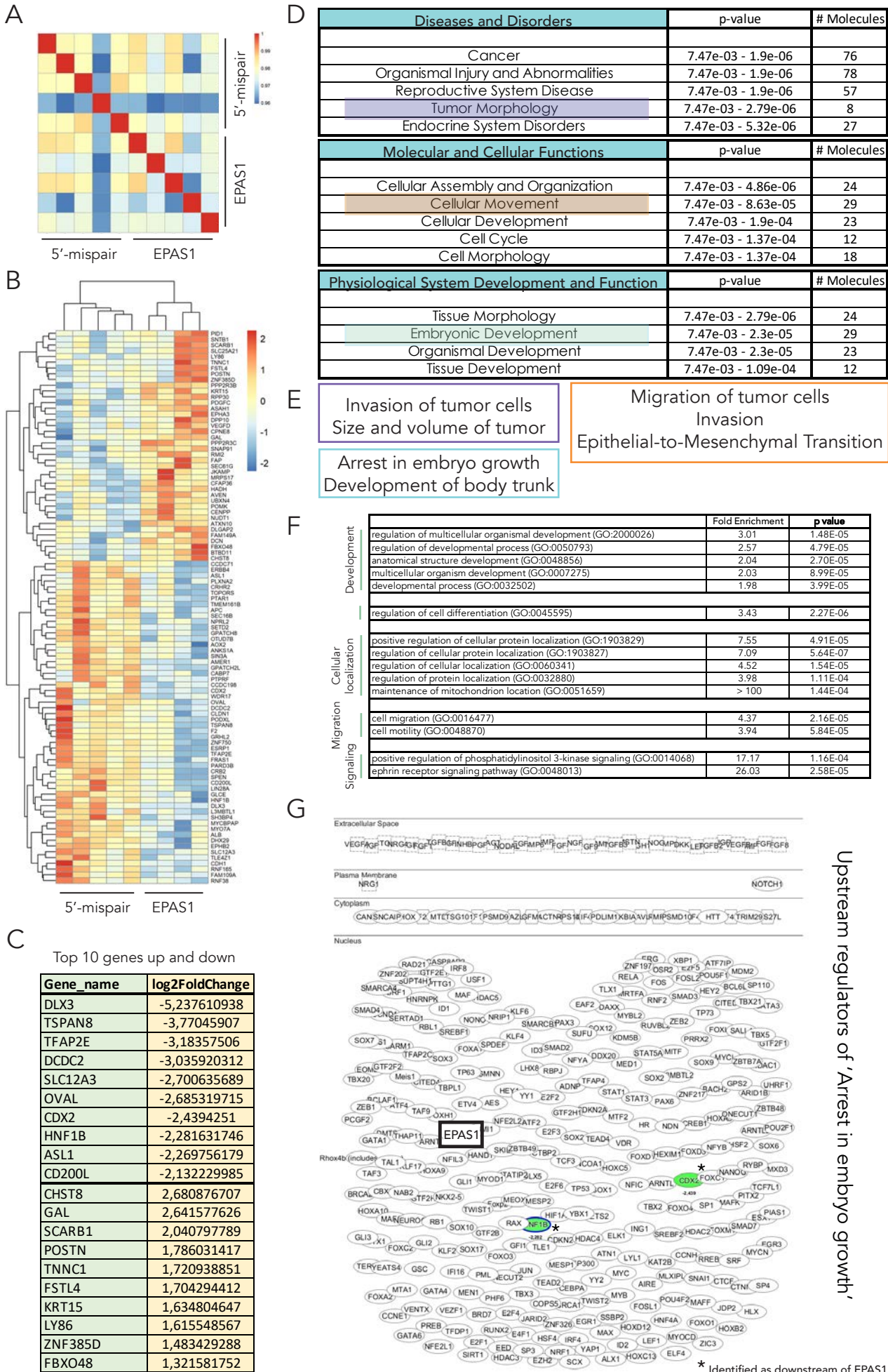


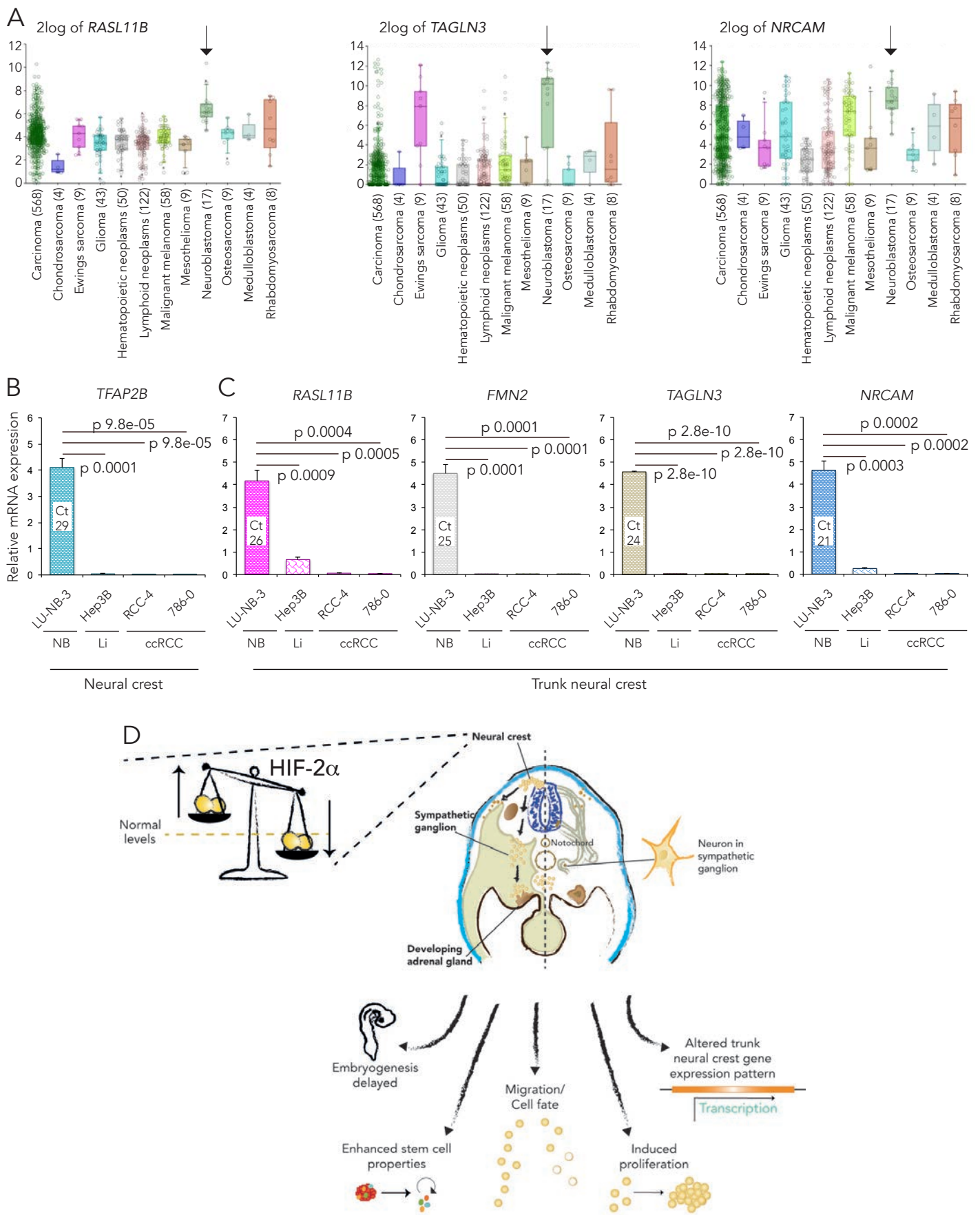
Figure 4











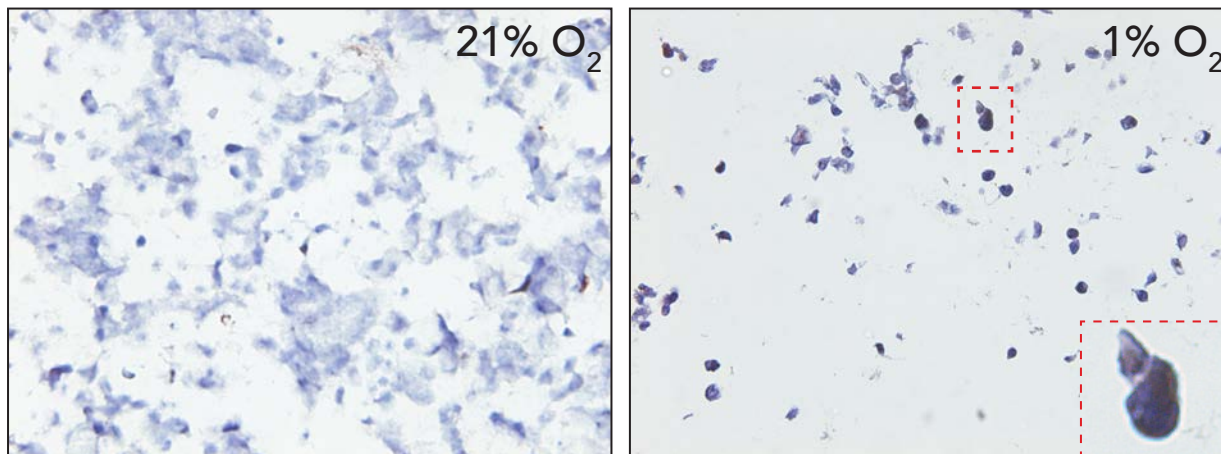
A.

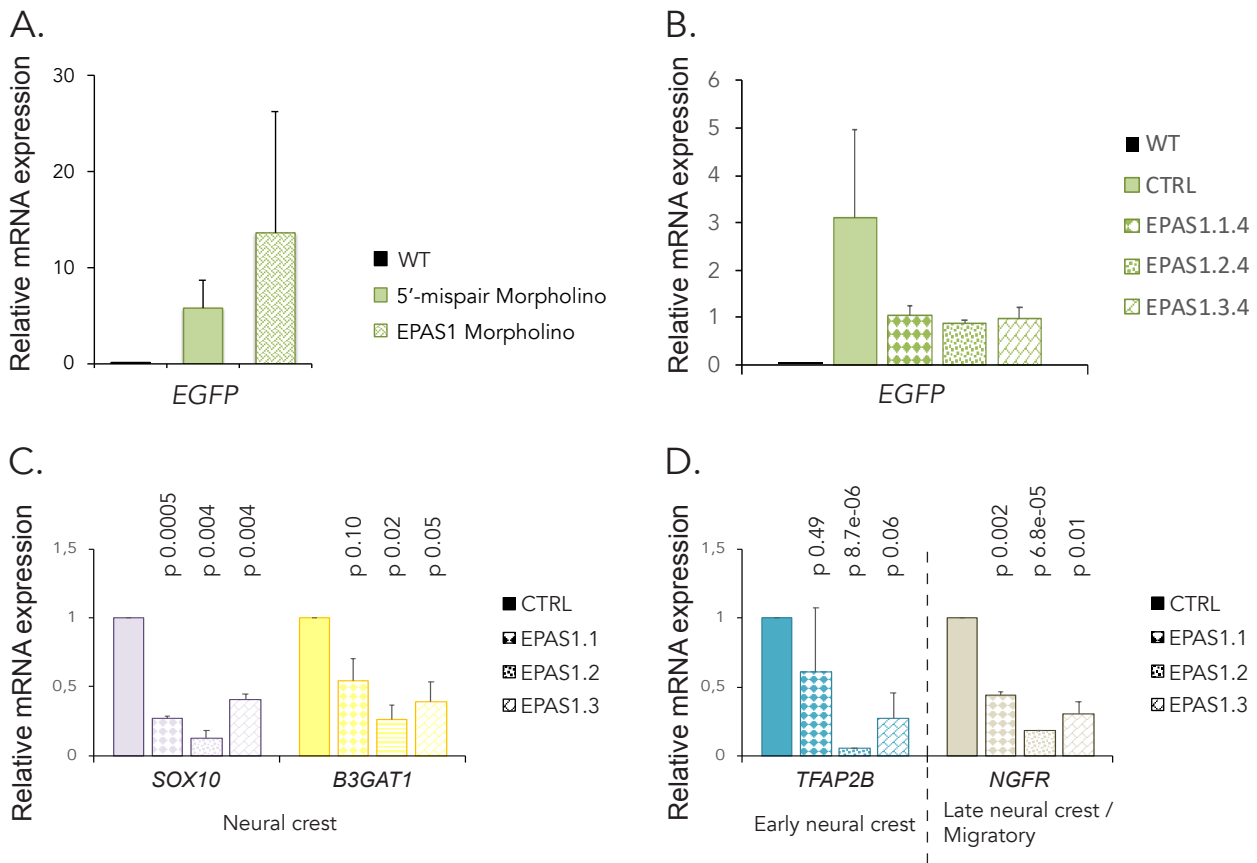
HIF-2 α staining control



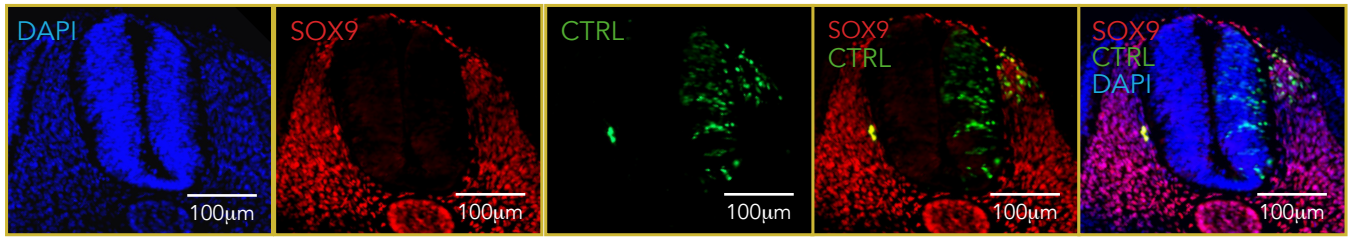
B.

SK-N-BE(2)c



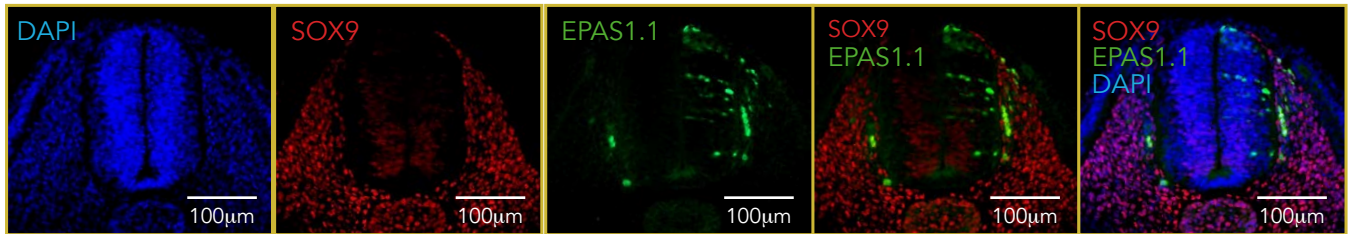


A.



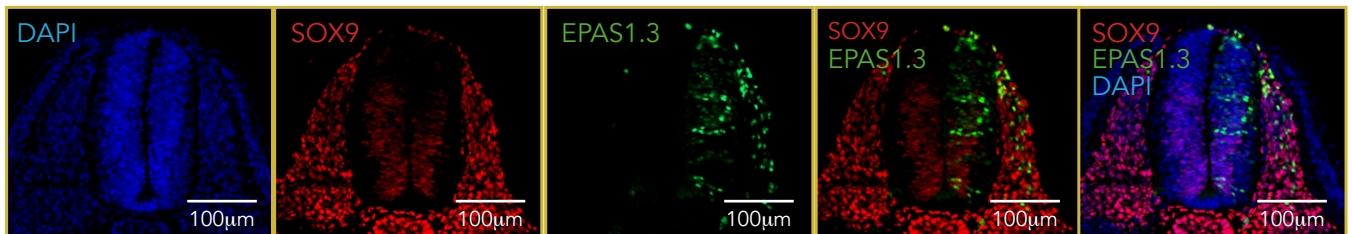
Control Electroporated

B.



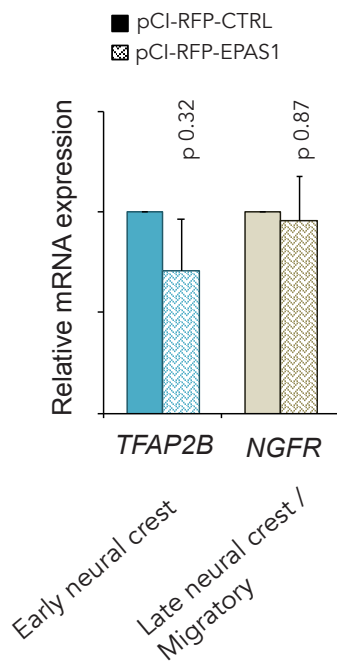
Control Electroporated

C.

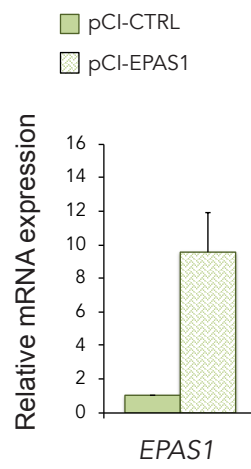


Control Electroporated

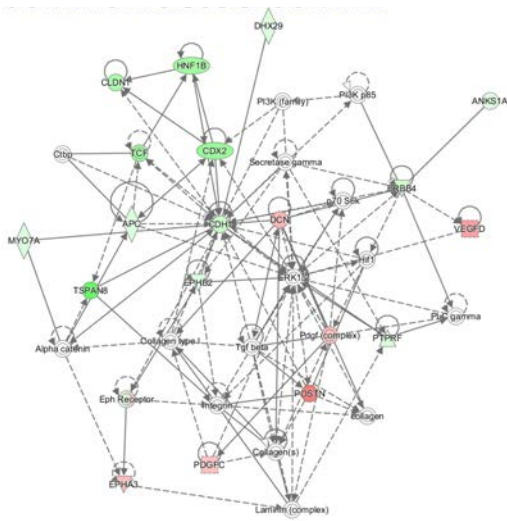
A.



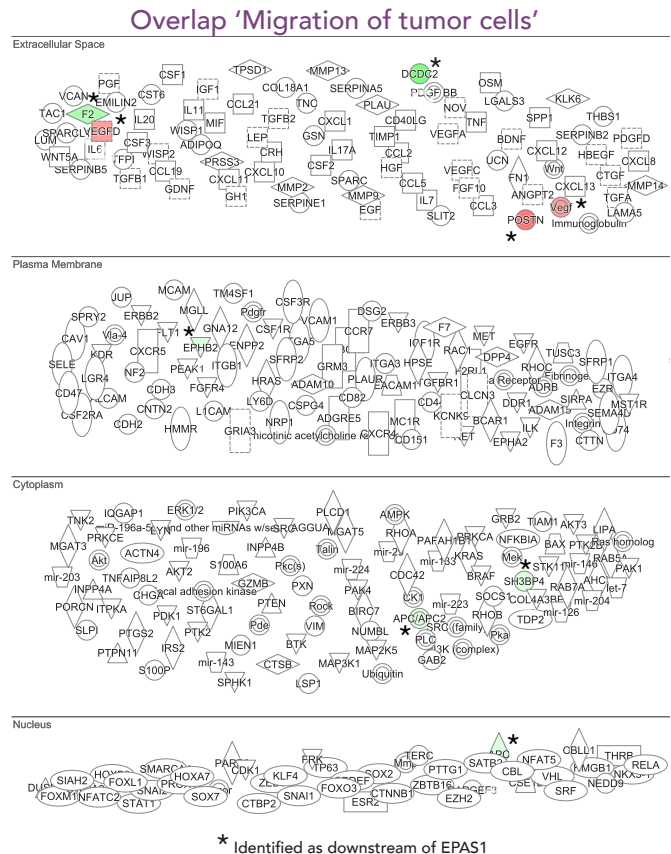
B.



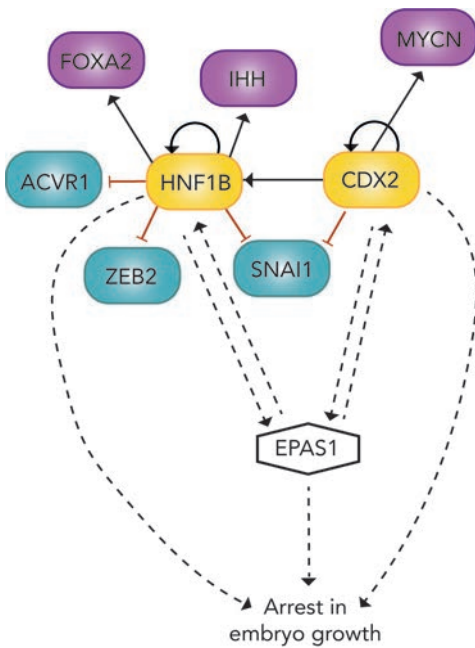
A.



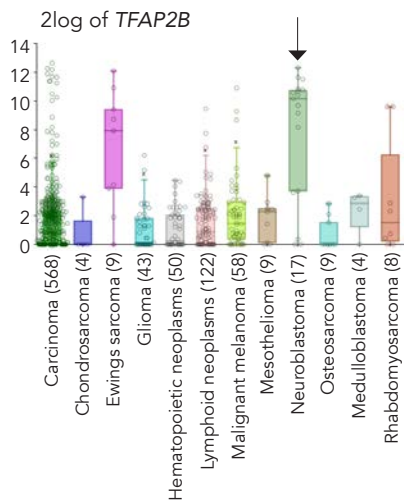
B.



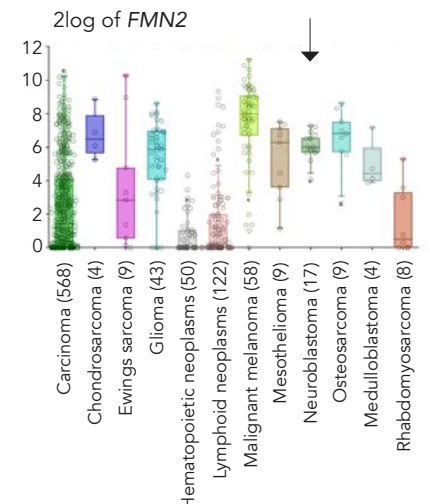
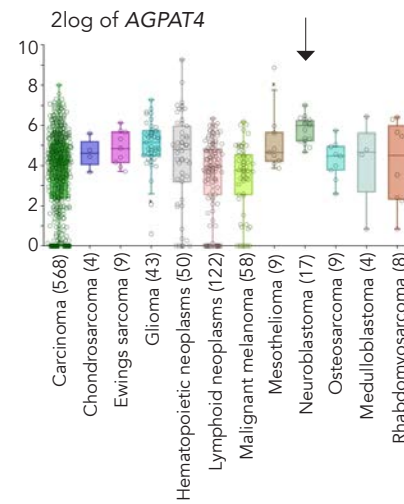
C.



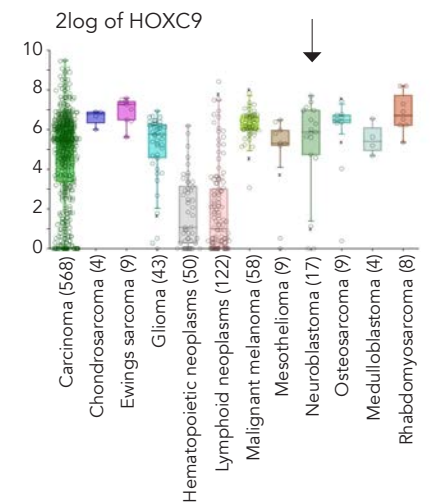
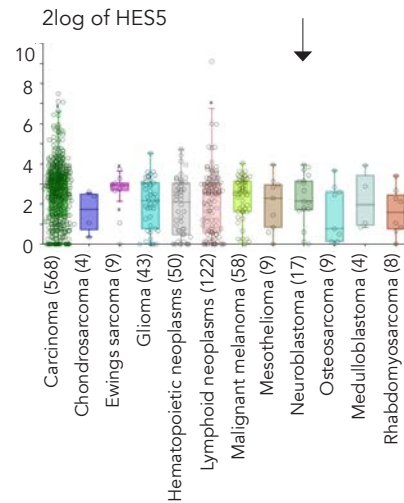
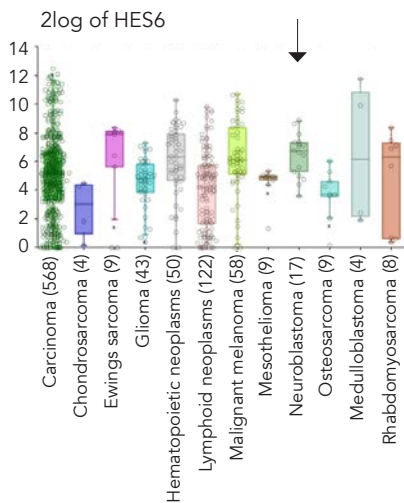
A. Neural crest



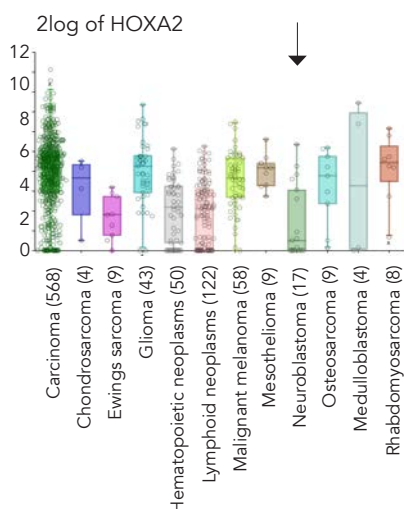
B. Trunk neural crest



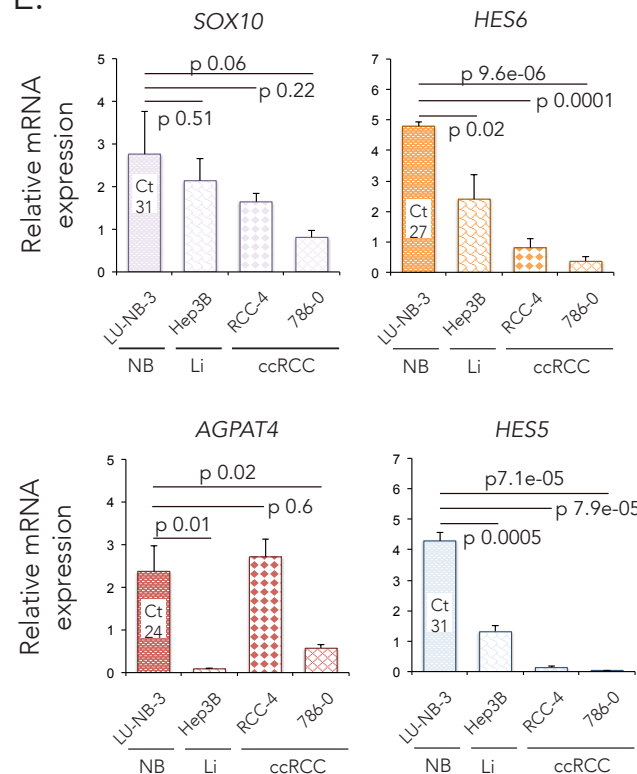
C. Trunk neural crest



D. Cranial neural crest



E.



Gene_stable_ID	Gene_name	log2FoldChange	p value
ENSGALG00000035219	ALB	-1.117182632	0.004326406
ENSGALG00000007599	AMER1	-0.405238741	0.000373362
ENSGALG00000002723	ANKS1A	-0.620471912	0.002221987
ENSGALG00000020876	AOX2	-1.096918485	0.00085007
ENSGALG00000000220	APC	-0.47416616	0.000273889
ENSGALG00000026364	ASAH1	0.421872055	0.002627088
ENSGALG00000002558	ASL1	-2.269756179	0.000254935
ENSGALG00000014234	ATXN10	0.477982264	0.001858816
ENSGALG00000009642	AVEN	0.319184758	0.002524998
ENSGALG00000039595	BTBD11	1.074785502	0.000312368
ENSGALG00000040463	CABP7	-1.850580177	0.003025143
ENSGALG00000012095	CCDC198	-1.657954928	0.00269933
ENSGALG00000006787	CCDC71	-0.470629203	0.002673943
ENSGALG00000015395	CD200L	-2.132229985	0.000154209
ENSGALG00000000608	CDH1	-1.307331812	0.000773978
ENSGALG00000034983	CDX2	-2.4394251	8.25E-05
ENSGALG00000004687	CENPP	0.424109009	0.000169658
ENSGALG00000037504	CFAP36	0.393170817	0.00331114
ENSGALG00000004903	CHST8	2.680876707	0.004291268
ENSGALG00000028662	CLDN1	-1.995178284	0.00010847
ENSGALG00000007025	CPNE8	1.148105385	0.004533116
ENSGALG00000001169	CRB2	-0.810451518	0.001196479
ENSGALG00000005657	CRHR2	-0.937081004	0.004656735
ENSGALG00000042454	DCDC2	-3.035920312	0.003127781
ENSGALG00000011274	DCN	0.981364002	0.002209936
ENSGALG00000014700	DHX29	-0.444692933	0.003215344
ENSGALG00000032937	DLGAP2	1.296643213	0.003793901
ENSGALG00000040529	DLX3	-5.237610938	0.001107996
ENSGALG00000012156	DPP10	1.123811132	0.001713737
ENSGALG00000015403	EPHA3	0.860641014	0.001951451
ENSGALG00000004741	EPHB2	-0.418815561	0.001893072
ENSGALG00000003126	ERBB4	-1.15424847	0.001506512
ENSGALG00000031076	ESRP1	-1.882592181	0.001558762
ENSGALG00000008332	F2	-1.908762077	0.001551013
ENSGALG000000041153	FAM109A	-1.215286589	0.004594595
ENSGALG00000013503	FAM149A	0.797519339	0.004470883
ENSGALG00000011099	FAP	1.014306518	0.00201386
ENSGALG00000008753	FBXO48	1.321581752	0.002069094
ENSGALG00000010316	FRAS1	-0.558639554	0.001060929
ENSGALG00000031487	FSTL4	1.704294412	0.004365436
ENSGALG00000007047	GAL	2.641577626	0.001941927
ENSGALG00000028191	GLCE	-0.598344895	0.000897534
ENSGALG00000010350	GPATCH2L	-0.487810446	7.98E-06
ENSGALG00000041556	GPATCH8	-0.317242944	0.003590909
ENSGALG00000037687	GRHL2	-1.807620277	0.003321608
ENSGALG00000016124	HADH	0.25603248	0.003556043
ENSGALG00000005504	HNF1B	-2.281631746	0.00080264

ENSGALG00000012009	JKAMP	0.382527526	0.003435274
ENSGALG00000019718	KRT15	1.634804647	0.000760169
ENSGALG00000030710	L3MBTL1	-0.530953634	0.001495242
ENSGALG00000036022	LIN28A	-1.38546498	0.000196313
ENSGALG00000012801	LY86	1.615548567	0.003593197
ENSGALG00000002379	MIRP517	0.239466428	0.001783389
ENSGALG00000007661	MYCBPAP	-0.506429259	0.004333666
ENSGALG00000031450	MYO7A	-0.679727815	0.003592535
ENSGALG00000002131	NPRL2	-0.499654709	0.003409913
ENSGALG00000004245	NUDT1	0.510897854	0.00012546
ENSGALG00000013348	OTUD7B	-0.376188595	0.001170227
ENSGALG00000012869	OVAL	-2.685319715	0.002991518
ENSGALG00000042645	PARD3B	-0.501189766	1.96E-06
ENSGALG00000009378	PDGFC	0.796369213	0.001886551
ENSGALG00000002963	PID1	1.07251355	0.003711941
ENSGALG00000001264	PLXNA2	-0.787868279	0.002137423
ENSGALG00000006409	PODXL	-0.886446619	0.004450686
ENSGALG000000026210	POMK	0.337221928	0.003042971
ENSGALG00000017046	POSTN	1.786031417	0.004588475
ENSGALG00000016702	PPP2R3B	0.391820083	0.003451236
ENSGALG00000010052	PPP2R3C	0.399540693	0.001962875
ENSGALG00000015113	PTAR1	-0.539683505	0.001225948
ENSGALG00000010053	PTPRF	-0.480481292	0.003964241
ENSGALG00000007155	RM12	1.140626082	0.001382943
ENSGALG00000031018	RNF165	-1.03414841	0.001120092
ENSGALG00000015311	RNF38	-0.537721584	0.003385081
ENSGALG00000006486	RPP30	0.342750725	0.004109447
ENSGALG00000046226	SCARB1	2.040797789	0.00121797
ENSGALG00000004424	SEC16B	-1.1085265	0.000492445
ENSGALG00000037863	SEC61G	0.557099237	0.002778043
ENSGALG00000042051	SETD2	-0.308714867	0.000307483
ENSGALG00000004140	SH3BP4	-0.494833722	0.001195274
ENSGALG00000001644	SIN3A	-0.319985031	0.001157216
ENSGALG00000002957	SLC12A3	-2.700635689	0.000223534
ENSGALG00000010117	SLC25A21	0.766964291	0.00238367
ENSGALG00000015846	SNAP91	1.1198235	0.000304383
ENSGALG00000034528	SNTB1	1.15258033	0.003458367
ENSGALG00000036932	SPEN	-0.388461063	0.00077178
ENSGALG00000039497	TFAP2E	-3.18357506	0.000779405
ENSGALG00000015184	TLE4Z1	-0.444405062	0.001437148
ENSGALG00000010896	TMEM161B	-0.546018409	0.001173125
ENSGALG00000001459	TNNC1	1.720938851	0.003720707
ENSGALG00000020523	TOPORS	-0.473621698	0.003381281
ENSGALG00000010152	TSPAN8	-3.77045907	0.002947966
ENSGALG00000012259	UBXN4	0.264129274	0.004330698
ENSGALG00000043106	WDR17	-1.478943795	0.001766045
ENSGALG00000016558	VEGFD	1.266960804	0.004105067
ENSGALG00000011283	ZNF385D	1.483429288	0.004653997
ENSGALG00000001518	ZNF750	-1.901269846	0.002582973

	Fold Enrichment	p value
cytolysis by symbiont of host cells (GO:0001897)	> 100	1.44E-04
hemolysis in other organism involved in symbiotic interaction (GO:0052331)	> 100	1.44E-04
cytolysis in other organism involved in symbiotic interaction (GO:0051801)	> 100	2.30E-06
maintenance of mitochondrion location (GO:0051659)	> 100	1.44E-04
trans-synaptic signaling by trans-synaptic complex, modulating synaptic transmission (GO:0099557)	> 100	1.44E-04
hemolysis in other organism (GO:0044179)	> 100	1.44E-04
hemolysis by symbiont of host erythrocytes (GO:0019836)	> 100	1.44E-04
killing of cells in other organism involved in symbiotic interaction (GO:0051883)	> 100	4.01E-06
disruption of cells of other organism involved in symbiotic interaction (GO:0051818)	> 100	4.01E-06
cytolysis in other organism (GO:0051715)	> 100	4.01E-06
multi-organism cellular process (GO:0044764)	60.51	3.21E-05
cytolysis (GO:0019835)	55.01	4.07E-05
disruption of cells of other organism (GO:0044364)	50.43	5.06E-05
killing of cells of other organism (GO:0031640)	50.43	5.06E-05
axonal fasciculation (GO:0007413)	40.34	8.99E-05
neuron projection fasciculation (GO:0106030)	40.34	8.99E-05
ephrin receptor signaling pathway (GO:0048013)	26.03	2.58E-05
positive regulation of phosphatidylinositol 3-kinase signaling (GO:0014068)	17.17	1.16E-04
positive regulation of cellular protein localization (GO:1903829)	7.55	4.91E-05
regulation of cellular protein localization (GO:1903827)	7.09	5.64E-07
regulation of cellular localization (GO:0060341)	4.52	1.54E-05
cell migration (GO:0016477)	4.37	2.16E-05
cell motility (GO:0048870)	3.98	1.11E-04
regulation of protein localization (GO:0032880)	3.94	5.84E-05
localization of cell (GO:0051674)	3.94	5.84E-05
locomotion (GO:0040011)	3.73	2.39E-05
regulation of cell differentiation (GO:0045595)	3.43	2.27E-06
regulation of response to stimulus (GO:0048583)	3.01	1.48E-05
regulation of biological process (GO:0050789)	2.61	3.94E-05
regulation of cellular component organization (GO:0051128)	2.57	4.79E-05
regulation of multicellular organismal process (GO:0051239)	2.55	1.41E-05
positive regulation of cellular process (GO:0048522)	2.33	1.37E-05
positive regulation of biological process (GO:0048518)	2.27	1.36E-05
negative regulation of cellular process (GO:0048523)	2.25	7.91E-05
negative regulation of biological process (GO:0048519)	2.09	5.55E-06
cytolysis by symbiont of host cells (GO:0001897)	2.06	2.05E-06
regulation of multicellular organismal development (GO:2000026)	2.04	2.70E-05
regulation of developmental process (GO:0050793)	2.03	8.99E-05
anatomical structure development (GO:0048856)	2.02	6.47E-05
multicellular organism development (GO:0007275)	1.98	3.99E-05
developmental process (GO:0032502)	1.97	6.32E-05
positive regulation of metabolic process (GO:0009893)	1.85	3.35E-05
regulation of metabolic process (GO:0019222)	1.47	1.21E-04
positive regulation of cellular metabolic process (GO:0031325)	> 100	1.44E-04

IF antibodies				
Primary Antibody	Species	Dilution	Source	Product #
HNK1	Mouse	1:5	Hybridoma bank	3H5
HIF-2 α	Rabbit	1:50	Abcam	ab199
SOX9	Rabbit	1:1000	Millipore	ab5535
Secondary Antibody	Species	Dilution	Source	Product #
Anti-Mouse Alexa Fluor-594	Goat	1:1000	Invitrogen	A-11032
Anti-Rabbit Alexa Fluor-546	Donkey	1:1000 / 1:500	Invitrogen	A-10040
Anti-Mouse Alexa Fluor-488	Goat	1:1000	Invitrogen	A-11008

IHC antibodies				
Primary Antibody	Species	Dilution	Source	Product #
HIF-2 α	Mouse	1:1000	Novus Biologicals	NB100-132
HIF-2 α	Rabbit	1:4000	Abcam	ab199
TH	Rabbit	1:1600	Abcam	ab112

In situ antibodies				
	Species	Dilution	Source	Product #
Anti-dig-AP	Mouse	1:2000	Roche Diagnostics	11093274910

Nuclear staining				
	Species	Dilution	Source	Product #
DAPI		1:3000	Dako	D3571

Western blot antibodies				
Primary Antibody	Species	Dilution	Source	Product #
HIF-2 α	Rabbit	1:200	Abcam	ab199
SDHA	Mouse	1:4000	Abcam	ab14715
Secondary Antibody	Species	Dilution	Source	Product #
Anti-Rabbit	Monkey	1:3000	Invitrogen	65-6120
Anti-Mouse	Sheep	1:5000	Invitrogen	62-6520

AVIAN

Target gene		5' - 3'
<i>18S (Reference gene)</i>	Fwd	CCATGATTAAGGGGACGGC
	Rev	TGGCAAATGCTTTCGCTTT
<i>28S (Reference gene)</i>	Fwd	GGTATGGCCCGACGCT
	Rev	CCGATGCCGACGCTCAT
<i>EPAS1</i>	Fwd	GGCACCAATACCATGACGA
	Rev	CATGTGCGCGTAACTGTCC
<i>SOX10</i>	Fwd	AGCCAGCAATTGAGAAGAAGG
	Rev	GAGGTGCGAAGAGTTGTCC
<i>B3GAT1</i>	Fwd	TTGTGGAGGTGGTGAGGA
	Rev	GGCTGTAGGTGGGTGTAATG
<i>TFAP2B</i>	Fwd	CCCTCCAAAATCCGTTACTT
	Rev	GGGGACAGAGCAGAACACCT
<i>HOXC9</i>	Fwd	TAAGCCACGAAAACGAAGAG
	Rev	GAAGGAAAGTCGGCACAGTC
<i>HOXA2</i>	Fwd	AGGCAAGTGAAGGTCTGGTT
	Rev	TCGCCGTTCTGGTTCTCC
<i>NGFR</i>	Fwd	AGCAGGAGGAGGTGGAGAA
	Rev	CCCGTGTGAAGCAGTCTATG
<i>HES6</i>	Fwd	GCTGATGGCTGATTCCAAAG
	Rev	TCGCAGGTGAGGAGAAGGT
<i>AGPAT4</i>	Fwd	TGCTGGGCGTTCTAAATGG
	Rev	ACACTCCTGCTCATCTTCTGG
<i>HES5</i>	Fwd	GTATGCCTGGTGCCTCAAA
	Rev	GCTTGTGACCTCTGGAAATG
<i>RASL11B</i>	Fwd	GCTGGGCTGTGCTTTCTATG
	Rev	GGTGCTGGTGGTCTGTTGTT
<i>FMN2</i>	Fwd	CCATCAGCCAGTCAAGAGGA
	Rev	TAAAGCATCGGGAGCCAAAC
<i>TAGLN3</i>	Fwd	AGGCAGCATTCCAGACC
	Rev	ATGGGTTGTTCCCTTTG
<i>NRCAM</i>	Fwd	TCATTCCGTGTGATTGCTGT
	Rev	AAGGATTTTCATCGGGGTTT
<i>EGFP</i>	Fwd	CCGACCACTACCAGCAGAAC
	Rev	TTGGGGTCTTTGCTCAGG

HUMAN

Target gene		5' - 3'
<i>UBC (Reference gene)</i>	Fwd	ATTTGGGTCGCGGTTCTTG
	Rev	TGCCTTGACATTCTCGATGGT
<i>YWHAZ (Reference gene)</i>	Fwd	ACTTTTGGTACATTGTGGCTTCAA
	Rev	CCGCCAGGACAAACCAGTAT
<i>SDHA (Reference gene)</i>	Fwd	TGGGAACAAGAGGGCATCTG
	Rev	CCACCACTGCATCAAATTCATG
<i>SOX10</i>	Fwd	GGGCAAGGTCAAGAAGGAG
	Rev	ACCAGCGTCCAGTCGTAG
<i>TFAP2B</i>	Fwd	ACGACCCTACTCCCTGAAC
	Rev	TCCGAACCCACTTCTTGC
<i>HES6</i>	Fwd	ATGAGGACGGCTGGGAGA
	Rev	GCAGGCTCTCGTTGATCC
<i>AGPAT4</i>	Fwd	GCTTCTCACTCTCCTCTCTG
	Rev	ACCCTCCAGCAGCATCAC
<i>HES5</i>	Fwd	TGGAGAAGGCCGACATCCT
	Rev	GGCGACGAAGGCTTTGC
<i>RASL11B</i>	Fwd	CGGTTCTCACCAAACGA
	Rev	GGACCTGAATACCTGGAGTG
<i>FMN2</i>	Fwd	ATCCCTTCTGTGGTCTGCT
	Rev	AGTGTTCGTGGCTGGTTTG
<i>TAGLN3</i>	Fwd	GCAAATCTCCCAGTTCCTAAA
	Rev	TGTCCTTCCCTCCCATAGA
<i>NRCAM</i>	Fwd	GCCATCCACCATACCATTTT
	Rev	ATCAAGGTCCCATCCTCTCC

A.

Stem cell associated genes

Upstream Regulator	Molecule Type	p-value of overlap
SOX2	transcription regulator	3,72E-16
POU5F1 / OCT4	transcription regulator	5,29E-16
E2F4	transcription regulator	2,66E-12
KLF4	transcription regulator	2,61E-11
NANOG	transcription regulator	2,81E-07
EZH2	transcription regulator	2,69E-08
GLI1	transcription regulator	1,68E-05
NOTCH1	transcription regulator	2,31E-03
KLF2	transcription regulator	3,00E-03
SALL4	transcription regulator	1,67E-02
HEY1	transcription regulator	1,97E-02
KLF6	transcription regulator	2,66E-02
HEY2	transcription regulator	3,57E-02
BMI1	transcription regulator	2,84E-04

B.

BMP signaling associated genes

Upstream Regulator	Molecule Type	p-value of overlap
BMP4	growth factor	5,74E-11
BMP2	growth factor	2,69E-03
BMP10	growth factor	5,06E-03
BMP6	growth factor	1,17E-02
SMAD2	transcription regulator	5,66E-09
SMAD7	transcription regulator	8,82E-06
SMAD4	transcription regulator	5,43E-05
SMAD3	transcription regulator	1,38E-03

C.

Epithelial-to-Mesenchymal Transition (EMT) associated genes

Upstream Regulator	Molecule Type	p-value of overlap
SNAI1	transcription regulator	8,22E-04
ZEB2	transcription regulator	1,44E-03
TWIST1	transcription regulator	3,00E-03
ZEB1	transcription regulator	1,10E-02
LEF1	transcription regulator	2,03E-02
NODAL	growth factor	2,13E-02